

Recent advances in the internal functionalization of carbon nanotubes: synthesis, optical, and magnetic resonance studies

Ferenc Simon †, Rudolf Pfeiffer, and Hans Kuzmany

Institut für Materialphysik, Universität Wien

Strudlhofgasse 4, A-1090 Wien, Austria

ferenc.simon@univie.ac.at

Abstract

The hollow inside of single-wall carbon nanotubes (SWCNT) provides a unique degree of freedom to investigate chemical reactions inside this confined environment and to study the tube properties. It is reviewed herein, how encapsulating fullerenes, magnetic fullerenes, ^{13}C isotope enriched fullerenes and organic solvents inside SWCNTs enables to yield unprecedented insight into their electronic, optical, and interfacial properties and to study their growth. Encapsulated C_{60} fullerenes are transformed to inner tubes by a high temperature annealing. The unique, low defect concentration of inner tubes makes them ideal to study the effect of diameter dependent treatments such as opening and closing of the tubes. The growth of inner tubes is achieved from ^{13}C enriched encapsulated organic solvents, which shows that fullerenes do not have a distinguished role and it opens new perspectives to explore the in-the-tube chemistry. Encapsulation of magnetic fullerenes, such as $\text{N}@\text{C}_{60}$ and C_{59}N is demonstrated using ESR. Growth of inner tubes from ^{13}C enriched fullerenes provides a unique isotope engineered heteronuclear system, where the outer tubes contain natural carbon and the inner walls are controllably ^{13}C isotope enriched. The material enables to identify the vibrational modes of inner tubes which otherwise strongly overlap with the outer tube modes. The ^{13}C NMR signal of the material is specific for the small diameter SWCNTs. Temperature and field dependent ^{13}C T_1 studies show a uniform metallic-like electronic state for all inner tubes and a low energy, 3 meV gap is observed that is assigned to a long sought Peierls transition.

Contents

1	Introduction	3
2	Experimental methods and sample preparation	5
2.1	Sample preparation	5
2.2	Experimental methods	6
3	Results and discussion	7
3.1	Inner tubes in DWCNTs as local probes	7
3.1.1	Electronic and vibrational properties of DWCNTs	7
3.1.2	Phonon and quasi-particle life-times in DWCNTs	9
3.1.3	Probing the SWCNT diameter distribution through inner tube growth	11
3.1.4	Studying the reversible hole engineering using DWCNTs	12

3.2	Growth mechanism of inner tubes studied by isotope labeling	13
3.3	ESR studies on encapsulated magnetic fullerenes	17
3.4	NMR studies on isotope engineered heteronuclear nanotubes	21
4	Summary	24
5	Acknowledgements	24

1 Introduction

The era of nanotechnology received an enormous boost with the discovery of carbon nanotubes (CNTs) by Sumio Iijima in 1991 [1]. Before 1991 nano- and nanotechnology usually meant small clusters of atoms or molecules. The originally discovered CNTs contain several coaxial carbon shells and are called multi-wall CNTs (MWCNTs). Soon thereafter single-wall CNTs (SWCNTs), i.e. a carbon nanotube consisting of a single carbon shell were discovered [2, 3]. The principal interest in CNTs comes from the fact that they contain carbon only and all carbon are locally sp^2 bound, like in graphite, which provides unique mechanical and transport properties. This, combined with their huge, > 1000 , aspect ratio (the diameters being 1-20 nm and their lengths over a few micron or even exceeding cms) gives them an enormous application potential. The not exhaustive list of applications includes field-emission displays (exploiting their sharp tips) [4], cathode emitters for small sized x-ray tubes for medical applications [5], reinforcing elements for CNT-metal composites, tips for scanning probe microscopy [6], high current transmitting wires, cables for a future space elevator, elements of nano-transistors [7], and elements for quantum information processing [8].

Carbon nanotubes can be represented as rolled up graphene sheets, i.e. single layers of graphite. Depending on the number of coaxial carbon nanotubes, they are usually classified into multi-wall carbon nanotubes (MWCNTs) and single-wall carbon nanotubes (SWCNTs). Some general considerations have been clarified in the past 14 years of nanomaterial research related to these structures. MWCNTs are more homogeneous in their physical properties as the large number of coaxial tubes smears out individual tube properties. This makes them suitable candidates for applications where their nanometer size and the conducting properties can be exploited such as e.g. nanometer sized wires. In contrast, SWCNT materials are grown as an ensemble of weakly interacting tubes with different diameters. The physical properties of similar diameter SWCNTs can change dramatically as the electronic structure is very sensitive on the rolling-up direction, the so-called chiral vec-

tor [9, 10]. The chiral vector is characterized by the (n, m) vector components which denote the direction along which a graphene sheet is rolled up to form a nanotube. Depending on the chiral vector, SWCNTs can be metallic or semiconducting [10]. This provides a richer range of physical phenomena as compared to the MWCNTs, however significantly limits the range of applications. To date, neither the directed growth nor the controlled selection of SWCNTs with a well defined chiral vector has been performed successfully. Thus, their broad applicability is still awaiting. Correspondingly, current research is focused on the post-synthesis separation of SWCNTs with a narrow range of chiralities [11, 12, 13, 14] or on methods which yield information that are specific to SWCNTs with different chiralities. Examples for the latter are the observation of chirality selective band-gap fluorescence in semiconducting SWCNTs [15] and chirality assigned resonant Raman scattering [16, 17].

Clearly, several fundamental questions need to be answered before all the benefits of these novel nanostructures can be fully exploited. Recent theoretical and experimental efforts focused on the understanding of the electronic and optical properties of single-wall carbon nanotubes. It has been long thought that the one-dimensional structure of SWCNTs renders their electronic properties inherently one-dimensional [9, 10]. This was suggested to result in a range of exotic correlated phenomena such as the Tomonaga-Luttinger (TLL) state [18], the Peierls transition [19, 20], ballistic transport [21], and bound excitons [22, 23, 24, 25]. The presence of the TLL state is now firmly established [26, 27, 28], there is evidence for the ballistic transport properties [21] and there is growing experimental evidence for the presence of excitonic effects [29, 30]. The Peierls transition, however remains still to be seen.

An appealing tool to study the SWCNT properties originates from the discovery of fullerenes encapsulated inside SWCNTs by Smith, Monthioux, and Luzzi [31]. This peapod structure is particularly interesting as it combines two fundamental forms of carbon: fullerenes and carbon nanotubes. A high-resolution transmission electron microscopy (HR-TEM) image of a peapod is shown in Fig. 1. It was also shown that macroscopic filling with the

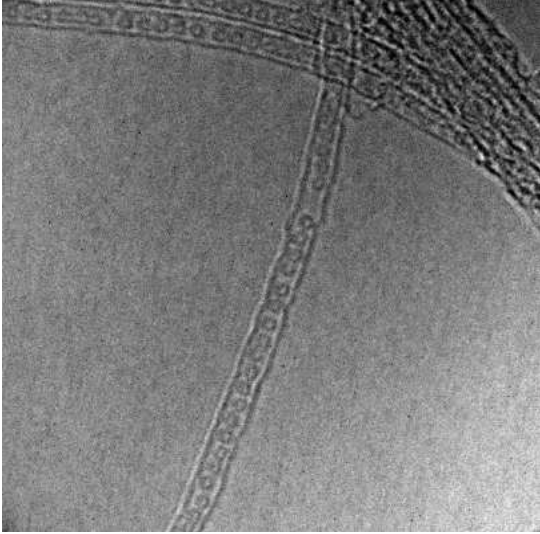


Figure 1: HR-TEM image of C_{60} @SWCNT peapods.

fullerenes can be achieved [32, 33]. This, in principle, opens the way to encapsulate magnetic fullerenes which would enable the study of the tube electronic properties using electron spin resonance as it is discussed in this review. Another interesting follow-up of the peapod structure discovery is that the encapsulated fullerenes can be fused into a smaller diameter inner tube [34, 35] thus producing a double-wall carbon nanotube (DWCNT). DWCNTs were first observed to form under intensive electron radiation [32] in a high resolution transmission electron microscope from C_{60} peapods. Following the synthesis of C_{60} peapods in macroscopic amounts [33], bulk quantities of the DWCNT material are available using a high temperature annealing method [35]. Alternatively, DWCNTs can be produced with usual synthesis methods such as arc-discharge [36] or CVD [37] under special conditions. According to the number of shells, DWCNTs are between SWCNTs and MWCNTs. Thus, one expects that DWCNTs may provide a material where improved mechanical stability as compared to SWCNTs coexists with the rich variety of electronic properties of SWCNTs. There are, of course, a number of yet unanswered questions

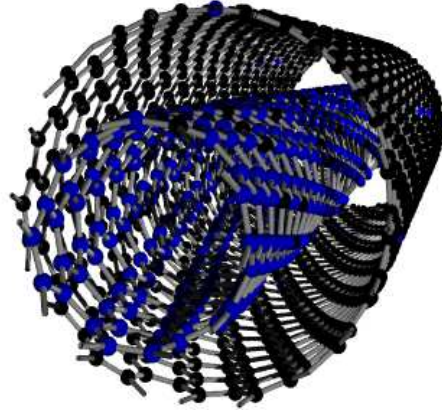


Figure 2: Schematic structure of an isotope engineered DWCNT with (14,6) outer and (6,4) inner tubes. ^{12}C and ^{13}C are shown in black and blue, respectively. The inner tube is 89 % ^{13}C enriched and the outer contains natural carbon (1.1 % ^{13}C abundance), which are randomly distributed for both shells.

e.g. if the outer tube properties are unaffected by the presence of the inner tube or if the commensurability of the tube structures plays a role. These questions should be answered before the successful application of these materials.

The inner tubes grown inside SWCNTs from peapods turned out to be a particularly interesting system as they are remarkably defect free which results in very long phonon life-times, i.e. very narrow vibrational modes [38]. In addition, their smaller diameters results in a larger energy spread, i.e. larger spectral splitting, for diameter dependent phonon modes such as e.g. the radial breathing mode (RBM). These two effects make the inner tubes very suitable to study diameter dependent physics of the small diameter tubes with precision. Here, we review how to employ the inner tubes as *probes* of the outer tube properties. The additional benefit of the inner tube growth from fullerenes is that the starting carbon

source can be tailored at wish, e.g. when ^{13}C isotope enriched fullerenes are encapsulated inside the SWCNT host tubes, ^{13}C isotope enriched inner tubes are grown. In Fig. 2 we show the schematics of such a DWCNT.

Here, we review the efforts to study the SWCNTs properties through encapsulation using Raman and magnetic resonance spectroscopy. The reviewed phenomena include the precise characterization of diameter distribution of SWCNTs, the study of reversible hole engineering on the SWCNTs, study of the inner tube growth mechanism with the help of ^{13}C isotope labeling, the study of local density of states on the tubes using nuclear magnetic resonance (NMR) on the ^{13}C isotope enriched inner tubes, and the electron spin resonance (ESR) studies of the SWCNTs using encapsulated magnetic fullerenes. This review is organized as follows. First, we present the general properties of DWCNTs using Raman, discuss the electronic and vibrational properties of the inner tubes, which are the probes in the subsequent studies. Second, we present the use of the inner tubes to probe the host outer tube diameter distribution and to study the opening and closing of holes on the outer tubes. Third, we present a study on the inner tube growth mechanism using isotope enriched carbon. Fourth, we discuss the efforts related to studying the SWCNT properties by encapsulating magnetic fullerenes using ESR. Fifth, we discuss the NMR results on the isotope enriched inner tubes and in particular we present the observation of a low energy spin-gap in the density of states of SWCNTs.

2 Experimental methods and sample preparation

2.1 Sample preparation

The starting SWCNT samples

SWCNTs from different sources and prepared by different methods were used. Commercial arc-discharge grown SWCNTs with 50 % weight purity (Nanocarblab, Moscow, Russia) and laser ablation prepared SWCNTs with 10 % weight purity

(Tubes@Rice, Houston, USA) were used. The latter material was purified through repeated steps of air oxidation and washing in HCl. Some laser ablation prepared and purified samples were obtained from H. Kataura. The purified samples are usually well opened to enable fullerene encapsulation. If not, annealing in air at 450 °C for 0.5 hour makes them sufficiently open. The HiPco samples used as reference were purchased from CNI (Carbon Nanotechnologies Inc., Houston, USA). Most samples were used in the form of a buckypaper, which is prepared by filtering a suspension of SWCNTs. We found that commercially available SWCNTs already meet a required standard in respect of purity and quality. In addition, for the amount of experimental work described here, reproducible samples i.e. a large amount of SWCNTs from similar quality, were required. Commercial samples meet this requirement, which compensates for their slightly inferior quality compared to laboratory prepared ones.

Synthesis of peapods

Encapsulation of fullerenes at low temperatures inside SWCNTs (solvent method) was performed by sonicating the fullerene and opened SWCNT suspensions together in organic solvents following Refs. [39, 40, 41, 42]. For fullerene encapsulation at high temperatures (the vapor method), the SWCNTs and the fullerenes were sealed under vacuum in a quartz ampoule and annealed at 650 °C for 2 hours [33]. Fullerenes enter the inside of the SWCNTs at this temperature due to their high vapor pressure that is maintained in the sealed environment. Non-encapsulated fullerenes were removed by dynamic vacuum annealing at the same temperature for 1 hour. High purity fullerenes were obtained from a commercial source (Hoechst AG, Frankfurt, Germany). The filling of SWCNTs with the fullerenes was characterized by observing the peapod structure in high-resolution transmission electron microscopy (HR-TEM), by x-ray studies of the one-dimensional array of fullerenes inside the SWCNTs and by the detection of the fullerene modes from the cages encapsulated inside the SWCNTs using Raman spectroscopy [33, 43].

Synthesis of DWCNTs

DWCNTs were prepared by two routes: from fullerene peapods and using chemical vapor deposition (CVD) growth technique [44]. The peapods were transformed to DWCNTs by a dynamic vacuum treatment at 1250 °C for 2 hours following Ref. [35]. Again, the DWCNT transformation was followed by HR-TEM and by the observation of the DWCNT structure factors using x-ray studies. In addition, new Raman modes emerge after the 1250 °C heat treatment particularly in a frequency range that is clearly upshifted from the outer tube RBMs. For the CVD DWCNT growth [44], the catalyst was a modified version of the Fe/Mo/MgO system developed by Liu *et al.* [45] for SWCNT synthesis.

Both kinds of DWCNTs have advantageous and disadvantageous properties. For peapod template grown DWCNTs, the inner tube is known to fill only up to $\sim 70\%$ of the outer tube length [46]. This is the consequence of insufficient carbon in the fullerenes: the C₆₀ peapods have 60 carbon atoms per 1 nm (the lattice constant of the peapod) whereas the (9,0) inner tube with $d = 0.708$, which is representative of the most abundant 7 nm diameter inner tube contains 36 carbon atoms per the $c_0 = 0.424$ nm lattice constant [47]. In contrast, CVD grown inner tubes fill up to the total length of the outer tubes, however such samples have usually a less well defined tube diameter distribution due to the inevitable growth of small diameter SWCNTs and large diameter DWCNTs [48]. Peapod template grown DWCNTs can be grown with relatively narrow diameter distribution due to the available narrow diameter distribution of the SWCNT host tubes. This also allows for a good control over the DWCNT diameter as described in Ref. [49] and is discussed below.

Synthesis of isotope engineered DWCNTs

Commercial ¹³C isotope enriched fullerenes (MER Corp., Tucson, USA) were used to prepare fullerene peapods C₆₀,C₇₀@SWCNT with enriched fullerenes. Two supplier specified grades of ¹³C enriched fullerene mixtures were used: 25 and 89 %, whose values were slightly refined based on the Raman spectroscopy. The 25 % grade was nominally C₆₀, and the

89 % grade was nominally C₇₀ with C₆₀/C₇₀/higher fullerene compositions of 75:20:5 and 12:88:< 1, respectively. The above detailed standard routes were performed for the peapod and the DWCNT productions.

2.2 Experimental methods

Raman spectroscopy

Raman spectra were measured with a Dilor xy triple spectrometer using various lines of an Ar/Kr laser, a He/Ne laser and a tunable Ti:sapphire and Rhodamin dye-laser in the 1.54-2.54 eV (805-488 nm) energy range. Tunable lasers allow to record the so-called Raman map [16, 17] i.e. to detect the SWCNT resonance energies through the Raman resonance enhancement [50], which ultimately allows the chiral index assignment. The spectra can be recorded in normal (NR) and high resolution (HR) mode, respectively ($\Delta\bar{\nu}_{\text{NR}} = 1.3\text{ cm}^{-1}$ for blue and $\Delta\bar{\nu}_{\text{HR}} = 0.4\text{ cm}^{-1}$ in the red). The samples in the form of bucky-paper are kept in dynamic vacuum and on a copper tip attached to a cryostat, which allows temperature variation in the 20-600 K temperature range. Raman spectroscopy was used to characterize the diameter distribution of the SWCNTs, to determine the peapod concentrations, and to monitor the DWCNT transformation of the peapod samples.

Electron spin resonance

The peapod and the reference SWCNT materials were mixed with the ESR silent high purity SnO₂ in a mortar to separate the pieces of the conducting bucky-papers. The samples were sealed under dynamic vacuum. A typical microwave power of 10 μW and 0.01 mT magnetic field modulation at ambient temperature were used for the measurements in a Bruker Elexsys X-band spectrometer.

Nuclear magnetic resonance

Nuclear magnetic resonance (NMR) is usually an excellent technique for probing the electronic properties at the Fermi level of metallic systems. The examples include conducting polymers, fullerenes,

and high temperature superconductors. However the 1.1% natural abundance of ^{13}C with nuclear spin $I=1/2$ limits the sensitivity of such experiments. As a result, meaningful NMR experiments have to be performed on ^{13}C isotope enriched samples. NMR data were taken with the samples sealed in quartz tubes filled with a low pressure of high purity Helium gas [51]. We probed the low frequency spin dynamics (or low energy spin excitations, equivalently) of the inner-tubes using the spin lattice relaxation time, T_1 , defined as the characteristic time it takes the ^{13}C nuclear magnetization to recover after saturation. The signal intensity after saturation, $M(t)$, was deduced by integrating the fast Fourier transform of half the spin-echo for different delay times, t .

3 Results and discussion

3.1 Inner tubes in DWCNTs as local probes

3.1.1 Electronic and vibrational properties of DWCNTs

Encapsulating fullerenes and transforming them into inner tubes by the high temperature annealing process [35] provides a unique opportunity to study the properties of the host outer tubes. In Fig. 3 we show the evolution of the SWCNT Raman spectrum upon C_{60} fullerene encapsulation and the DWCNT transformation after Ref. [38]. The series of sharp modes in the peapod spectrum, which are related to the encapsulated fullerenes [43], disappear upon the heat treatment and a series of sharp modes appear in the $250\text{-}450\text{ cm}^{-1}$ spectral range. The presence of inner tubes after this protocol have been independently confirmed by HR-TEM [34]. The small diameter tubes with $d \sim 0.7\text{ nm}$ would have RBM modes in the $\sim 250\text{-}450\text{ cm}^{-1}$ spectral range, which clarifies the identification of these modes. The identification of the inner tube RBMs is possible due to the strong d dependence of this Raman mode [52]. Assignment of less diameter dependent modes such as the G mode [10] to inner and outer tubes are more difficult although a number of small intensity new modes are observed for the DWCNT sample in Fig. 3. It is

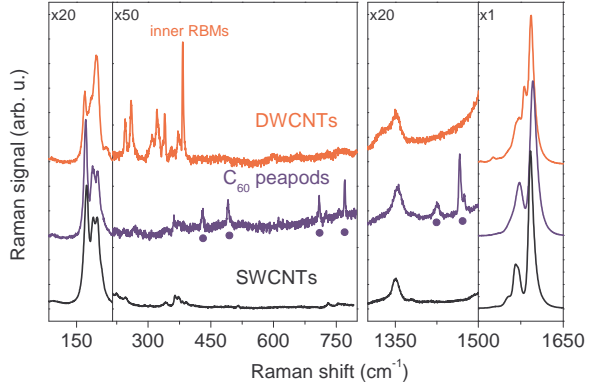


Figure 3: Transformation of fullerene peapods to DWCNTs as followed with Raman spectroscopy at 496.5 nm laser excitation and 90 K. The SWCNT Raman spectra (lower curve) is shown as reference. The fullerene related peapod modes (dots) in the middle curve disappear upon the heat treatment. Note the sharp RBMs appearing in the $250\text{-}450\text{ cm}^{-1}$ for the DWCNT sample.

shown in Section 3.2 that unambiguous assignment can be given with the help of selective isotope enrichment of the inner walls.

A variety of additional information can be gained about the inner tube properties when their RBMs are studied using the additive mode, i.e. high-resolution of the Raman spectrometer. In Fig. 4, we show the inner tube RBMs at 90 K with high-resolution in comparison with an SWCNT sample with similar tube diameter prepared by the HiPco process. Three striking observations are apparent in the comparison of the two spectra: i) there are a larger number of inner tube RBMs than geometrically allowed and they appear to cluster around the corresponding modes in the SWCNT sample, ii) the inner tube RBMs are on average an order of magnitude narrower than the SWCNT RBMs in the HiPco sample [38] and iii) the Raman intensity of the inner tubes is large in view of the ~ 3 times less number of carbon atoms on them [53]. Points ii) and iii) are explained by the long phonon and quasi-particle life-times of inner tubes

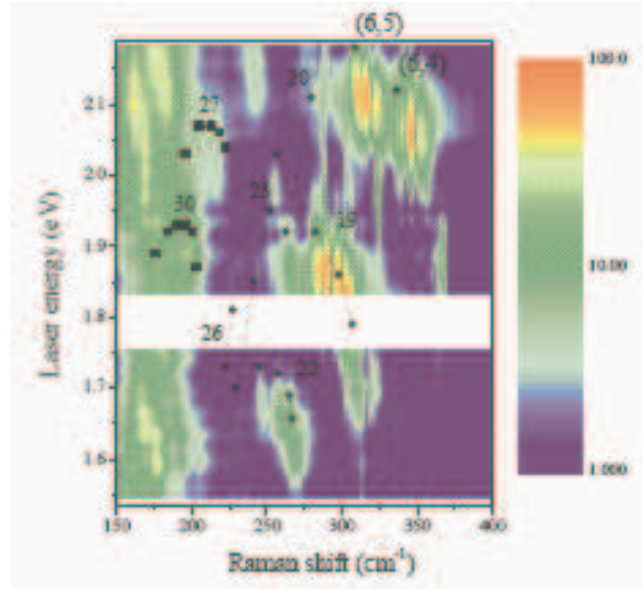
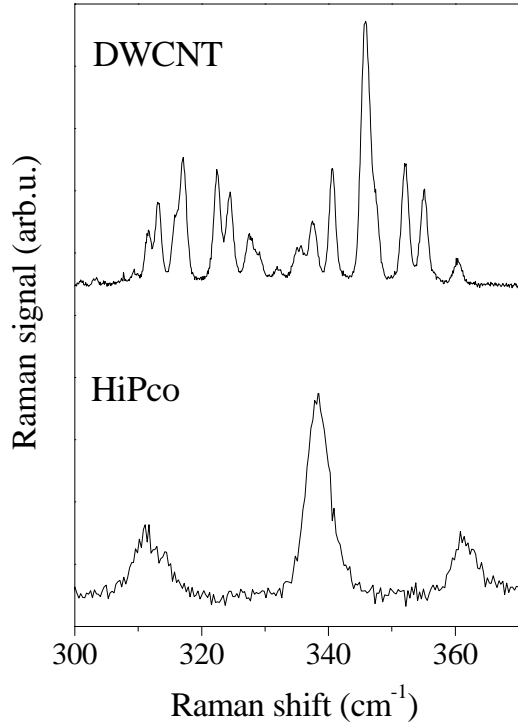


Figure 4: Raman spectra of the RBMs in DWCNT and HiPco (SWCNT) samples at 594 nm laser excitation and 90 K in the high resolution spectrometer mode.

which are discussed further below.

Observation i), i.e. the clustering behavior of the observed inner tube RBMs around SWCNT RBMs, is further evidenced in energy dispersive Raman measurements. In Fig. 5, we show the Raman map for the DWCNTs from Ref. [54]. The advantage of studying Raman maps is that the optical transition energies are also contained in addition to the Raman shifts. These two quantities uniquely identify the chirality of a nanotube [10, 55, 56]. The analogous Raman map for HiPco SWCNTs were measured by Fantini *et al.* [16] and Telg *et al.* [17]. Their results are also shown in Fig. 5) with squares and circles for metallic and semiconducting tubes, respectively. It turns out that family patterns with $2n + m = \text{const}$ can be

the same family. Laser excitation was not available in the missing area. Reprinted figure with permission from Ref. [54], R. Pfeiffer *et al.* Phys. Rev. B **72**, 161404 (2005). Copyright (2005) by the American Physical Society.

identified for which the tube resonance energies and Raman shifts are closely grouped together [15]. The comparison of the HiPco results and the DWCNT Raman map confirms the above statement, i.e. that a number of inner tube modes are observed for the DWCNT where only a few (or one) SWCNT chirality is present. This is best seen for the (6,5) and (6,4) chiralities which are well resolved from other modes.

In Fig. 6, we show the Raman maps for the two samples near the energy and Raman shift regions for the (6,5) and (6,4) tube modes [15, 16, 17]. The comparison of the Raman maps of the two kinds of samples shows that the corresponding tube modes are split into up to 15 components for the inner tube

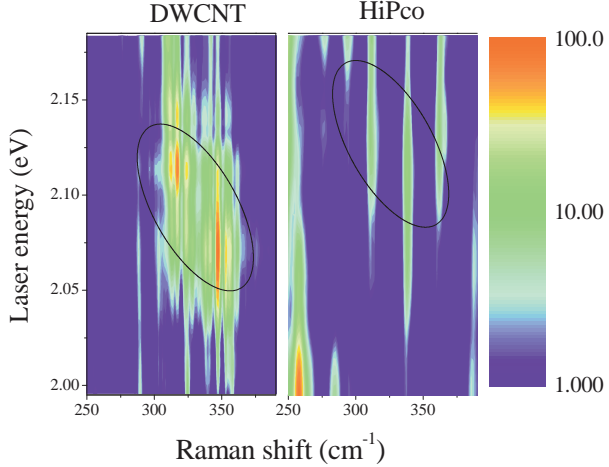


Figure 6: Raman map comparison of the (6,5) and (6,4) tube RBM ranges for DWCNT and SWCNT (HiPco) samples. Ellipsoids indicate the corresponding tube modes. Note the progressive transition energy downshift for the split components of the inner tubes and the 30 meV transition energy difference between the two kinds of samples, which are discussed in the text.

RBMs. This is explained by the inner-outer tube interaction in the DWCNT samples: an inner tube with a particular chirality can be grown in outer tubes with different diameters (chiralities). The varying inner-outer tube spacing can give rise to a different Raman shift for the split components. The large number of split components is a surprising result as it is expected that an inner tube with a given diameter is grown in maximum 1-2 outer tubes where its growth is energetically preferred.

To further prove the origin of the splitting and to quantify this effect, model calculations on the inner-outer tube interactions were performed [54, 57] following the continuum model of Popov and Henrard [58]. These calculations showed that the interaction of inner and outer tubes can give rise to a shift in the inner tube RBM frequency up to 30 cm^{-1} .

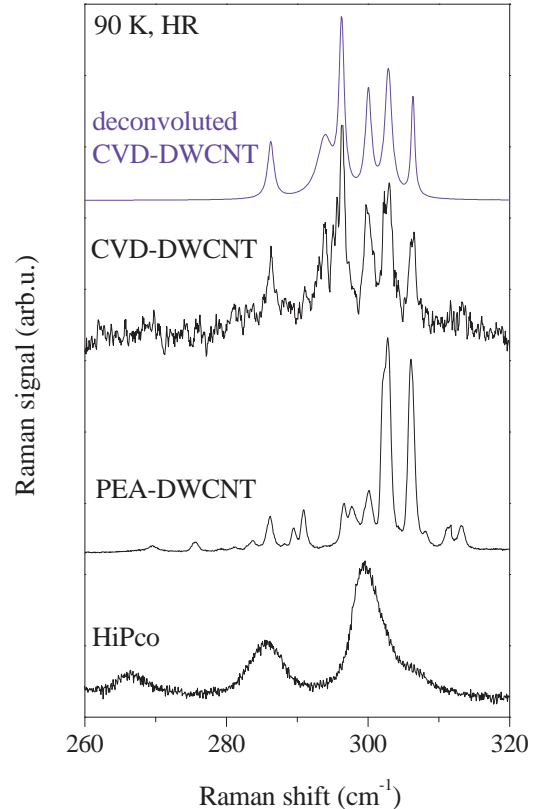


Figure 7: High resolution Raman spectra taken at 676 nm laser excitation and 90 K on the CVD- and PEA-DWCNT and an SWCNT reference (HiPco) sample. The deconvoluted spectrum is also shown for the CVD-DWCNT sample. The narrow line-widths indicate the long RBM phonon life-times of the inner tubes in both DWCNT materials. Reprinted figure with permission from Ref. [44], F. Simon *et al.* Chem. Phys. Lett. **413**, 506 (2005). Copyright (2005) by Elsevier.

3.1.2 Phonon and quasi-particle life-times in DWCNTs

Now, we turn to discussion of the observed very narrow line-widths of the RBMs. This is the most important property of the inner tube RBMs, which will

be exploited throughout in this work. Intrinsic line-widths can be determined by deconvoluting the experimental spectra with a Voigtian fit, whose Gaussian component describes the spectrometer resolution and the Lorentzian gives the intrinsic line-width. The Lorentzian component for some inner tube RBMs is as small as 0.4 cm^{-1} [38], which is an order of magnitude smaller than the values obtained for isolated individual tubes in a normal SWCNT sample [59]. The narrow line-widths, i.e. long phonon life-times of the inner tube RBMs was originally associated to the perfectness of the inner tubes grown from the peapod templates [38]. It was found, however, that inner tubes in chemical vapor deposition (CVD) grown DWCNTs have similarly small line-widths [44]. In Fig. 7, the high resolution spectra for the inner tube RBMs in CVD and peapod template grown DWCNTs is shown. This suggests, that the tube environment plays an important role in the magnitude of the observable RBM line-width.

The tube-tube interactions have been shown to give rise to up to $\approx 30 \text{ cm}^{-1}$ extra shift to the RBMs [54]. The principal difference between SWCNTs and inner tubes in DWCNTs (irrespective whether these are CVD or peapod template grown) is the different surrounding of a small diameter SWCNT with a given chirality: for the SWCNT sample, each tube is surrounded by the ensemble of other SWCNTs. For a close packed hexagonal bundle structure [60], this involves 6 nearest neighbors with random chiralities. This causes an inhomogeneous broadening of the RBMs. However, the nearest-neighbor of an inner tube with a given chirality is an outer tube also with a well defined chirality. A given inner tube can be grown in several outer tubes with different diameters, however the chiralities of an inner-outer tube pair is always well defined, therefore the nearest neighbor interaction acting on an inner tube is also well-defined.

In addition to the long phonon life-times of inner tubes, the life-time of optical excitations, i.e. the life-time of the quasi-particle associated with the Raman scattering is unexpectedly long. To demonstrate this, we compare the resonant Raman scattering data for an inner tube and a SWCNT with the same chirality following Ref. [61]. In Fig. 8 we show the energy pro-

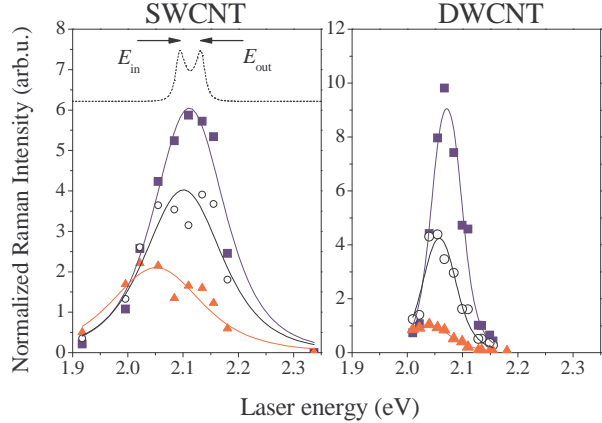


Figure 8: Raman resonance profile for the (6,4) tubes in the SWCNT (CoMoCat) and DWCNT samples, ■: 80 K, ○: 300 K, ▲: 600 K. Solid curves show fits with the RRS theory. Dashed curve is a simulation for the 80 K SWCNT data with $\Gamma = 10 \text{ meV}$. Arrows indicate the incoming and outgoing resonance energies. Note the much narrower widths for the DWCNT sample. Reprinted figure with permission from Ref. [61], F. Simon *et al.* Phys. Rev. B **74**, 121411(R) (2006). Copyright (2006) by the American Physical Society.

file of the resonant Raman scattering at some selected temperatures for two 6,4 tube modes: one is an inner tube in a DWCNT sample, the other is a SWCNT in a CoMoCat sample. Such energy profiles are obtained by taking an energy (vertical) cross section of a Raman map such as shown in Fig. 6. The Raman intensities for a given excitation energy were obtained by fitting the spectra with Voigtian curves for the tube modes, whose Gaussian component accounts for the spectrometer resolution and whose Lorentzian for the intrinsic line-width. For the DWCNT sample, the strongest (6,4) inner tube component at 347 cm^{-1} and for the SWCNT CoMoCat sample the (6,4) tube mode at 337 cm^{-1} is shown. The temperature dependent resonant Raman data can be fitted with the conventional resonance Raman theory for Stokes Raman modes [50, 62]:

$$I(E_l) = M_{\text{eff}}^4 \left| \frac{(E_l - E_{\text{ph}})^4 (n_{\text{BE}}(E_{\text{ph}}) + 1)}{(E_l - E_{\text{ii}} - i\Gamma) (E_l - E_{\text{ph}} - E_{\text{ii}} - i\Gamma)} \right|^2 \quad (1)$$

Here, the electronic density of states of SWCNTs is assumed to be a Dirac function and the effective matrix element, M_{eff} , describing the electron-phonon interactions is taken to be independent of temperature and energy. E_l , E_{22} and E_{ph} are the exciting laser, the optical transition and the phonon energies, respectively. $n_{\text{BE}}(E_{\text{ph}}) = (\exp(E_{\text{ph}}/k_B T) - 1)^{-1}$ is the Bose-Einstein function and accounts for the thermal population of the vibrational state [50] and $n_{\text{BE}}(E_{\text{ph}}) + 1$ changes a factor ~ 2 between 80 and 600 K. The temperature dependence of E_{ph} is $\sim 1\%$ for the studied temperature range [63] thus it can be neglected. The first and second terms in the denominator of Eq. 1 describe the incoming and outgoing resonances, respectively and are indicated on a simulated curve by arrows in Fig. 8. These are separated by E_{ph} . This means the apparent width of the resonance Raman data does not represent Γ .

Clearly, the resonance width is always smaller for the DWCNT than for the SWCNT sample. In other words, the life-time of the optically excited quasi-particle is longer lived for the DWCNT. The quasi-particle life-time is an important parameter for the application of carbon nanotubes in optoelectronic devices [24, 25]. As a result, DWCNTs appear to be superior in this respect than their one-walled counterparts.

3.1.3 Probing the SWCNT diameter distribution through inner tube growth

As discussed above, the Raman spectra of inner tubes have several advantages compared to that of the outer tubes: i) their RBMs have about a factor 2 times larger splitting due to the smaller diameters, ii) the line-widths are about 10 times narrower. The larger spectral splitting and narrower line-widths of the inner tube RBMs enable to characterize the inner tube diameter distribution with a spectral resolution that is about 20 times larger as compared to the analysis on the outer tubes. To prove that studying the

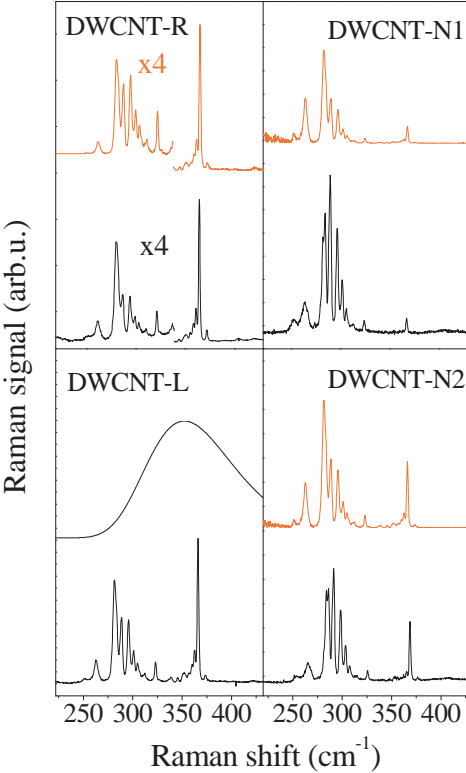


Figure 9: As measured Raman spectra of the inner nanotube RBMs for four DWCNT samples (lower curves in each quarter) at 647 nm laser excitation. The upper spectra (shown in red) are "smart-scaled" from the lower left spectrum. The Gaussian diameter distribution is shown for the DWCNT-L sample. Reprinted figure with permission from Ref. [49], F. Simon *et al.* Phys. Rev. B **71**, 165439 (2005). Copyright (2005) by the American Physical Society.

inner tubes can be exploited for the study of outer ones, here we show that there is a one-to-one correspondence between the inner and outer tube diameter distributions following Ref. [49].

In Fig. 9, we compare the inner tube RBM Raman spectra for four different DWCNT materials based on SWCNTs with different diameters and produced with different methods. The SWCNTs were

two arc-discharge grown SWCNTs (SWCNT-N1 and N2) and two laser ablation grown tubes (SWCNT-R and SWCNT-L). The diameter distributions of the SWCNT materials were determined from Raman spectroscopy [62] giving $d_{N1} = 1.50$ nm, $\sigma_{N1} = 0.10$ nm, $d_{N2} = 1.45$ nm, $\sigma_{N1} = 0.10$ nm, $d_R = 1.35$ nm, $\sigma_R = 0.09$ nm, and $d_L = 1.39$ nm, $\sigma_L = 0.09$ nm for the mean diameters and the variances of the distributions, respectively.

The spectra shown are excited with a 647 nm laser that is representative for excitations with other laser energies. The RBMs of all the observable inner tubes, including the split components [38], can be found at the same position in all DWCNT samples within the ± 0.5 cm⁻¹ experimental precision of the measurement for the whole laser energy range studied. This proves that vibrational modes of DWCNT samples are robust against the starting material.

As the four samples have different diameter distributions, the overall Raman patterns look different. However, scaling the patterns with the ratio of the distribution functions ("smart-scaling") allows to generate the overall pattern for all systems, starting from e.g. DWCNT-L in the bottom-left corner of Fig. 9. It was assumed that the inner tube diameter distributions follow a Gaussian function with a mean diameter 0.72 nm smaller than those of the outer tubes following Ref. [46] and with the same variance as the outer tubes. The empirical constants from Ref. [64] were used for the RBM mode Raman shift versus inner tube diameter expression. The corresponding Gaussian diameter distribution of inner tubes is shown for the DWCNT-L sample in Fig. 9. A good agreement between the experimental and simulated patterns for the DWCNT-R sample is observed. A somewhat less accurate agreement is observed for the DWCNT-N1, N2 samples, which may be related to the different growth method: arc discharge for the latter, as compared to laser ablation for the R and L samples. The observed agreement has important consequences for the understanding of the inner tube properties. As a result of the photoselectivity of the Raman experiment, it proves that the electronic structure of the inner tubes is identical in the different starting SWCNT materials.

The scaling of the inner tube Raman spectra with

the outer tube distribution shows that the inner tube abundance follows that of the outer ones. This agrees with the findings of x-ray diffractometry on DWCNTs [46] and is natural consequence of the growth of inner tubes inside the outer tube hosts.

3.1.4 Studying the reversible hole engineering using DWCNTs

Soon after the discovery of the peapods [31], it was recognized [33, 65] that opening the SWCNTs by oxidation in air or by treating in acids is a prerequisite for good filling. Good filling means a macroscopic filling where the peapods are observable not only by local microscopic means such as HR-TEM but also by spectroscopy such as Raman scattering. On the other hand, a heat treatment around 1000 °C was known to close the openings which results in a low or no fullerene filling. It was also shown that the geometrically possible maximum of filling can be achieved when purified SWCNTs were subject to a 450 °C heat treatment in flowing oxygen [66]. However, these studies have concerned the overall fullerene filling, with no knowledge on the precise dependence on the thermal treatment or tube diameter specificity.

The high diameter and chirality sensitivity of Raman spectroscopy for the inner tubes allows to study the behavior of tube openings when subject to different treatments. More precisely, openings which allow fullerenes to enter the tubes can be studied. This is achieved by studying the resulting inner tube RBM pattern when the outer tube host was subject to some closing or opening treatments prior to the fullerene encapsulation [67]. Annealing of as purchased or opened tubes was performed at various temperatures between 800 °C and 1200 °C in a sealed and evacuated quartz tube at a rest gas pressure of 10⁻⁶ mbar. Opening of the tubes was performed by exposure to air at various temperatures between 350 °C and 500 °C.

Figure 10 shows the Raman response of tubes after the standardized DWCNT transformation conditions but different pre-treatment. Only the spectral range of the inner tube is shown in the main part of the figure. The spectrum at the center was recorded under identical conditions but the SWCNT was pre-

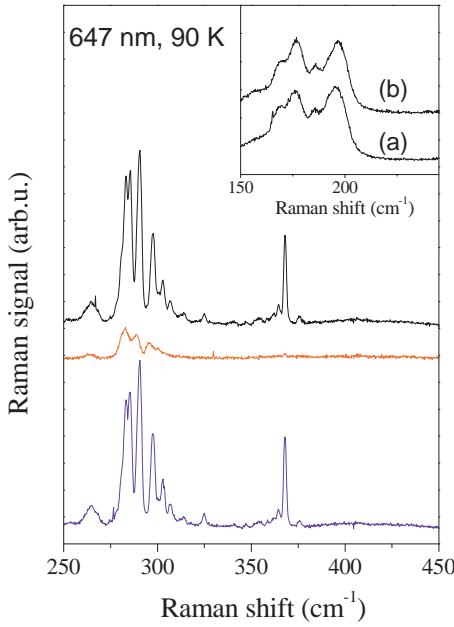


Figure 10: Raman spectra in the spectral range of the inner shell tube RBM for nanotubes after special pre-treatment. Bottom: after filling the tubes with C_{60} and standard transformation; Center: after annealing the tubes at $1000\text{ }^{\circ}\text{C}$, filling with C_{60} and standard transformation; Top: after re-opening the annealed samples, filling with C_{60} , and standard transformation. All spectra recorded at 90 K and $\lambda = 647\text{ nm}$. Insert: the RBM of the outer tubes before (a) and after (b) annealing at $1000\text{ }^{\circ}\text{C}$. Reprinted figure with permission from Ref. [67], F. Hasi *et al.* *J. Nanosci. Nanotechnol.* **5**, 1785 (2005). Copyright (2005) by the American Scientific Publishers.

annealed before the standardized filling and standardized transformation. Almost no response from inner shell tubes is observed for this material, which means no fullerenes had entered the tubes: the tubes were very efficiently closed by the annealing process. The insert in Fig. 10 depicts the RBM response from the outer tubes before and after annealing. The two spectra are almost identical, which proves that no outer tube coalescence had occurred at the temperature applied. The spectrum at the top in Fig. 10 was recorded after reopening the annealed tubes at $500\text{ }^{\circ}\text{C}$ on air and standard filling and transformation. The spectra derived from the pristine and from the reopened tubes are identical in all details. This means no dramatic damages by cutting a large number of holes into the sidewalls have happened. Consequently, the sidewalls of the tubes remain highly untouched by the opening process. Thus, it is suggested that fullerenes enter the tubes through holes at the tube ends.

3.2 Growth mechanism of inner tubes studied by isotope labeling

The growth of inner tubes from fullerenes raises the question, whether the fullerene geometry plays an important role in the inner tube growth or it acts as a carbon source only. Theoretical results suggest the earlier possibility [68, 69]. In addition, it needs clarification whether carbon exchange occurs between the two tube walls. Here, we review ^{13}C isotope labeled studies aimed at answering these two open questions. ^{13}C is a naturally occurring isotope of carbon with 1.1 % abundance. In general, isotope substitution provides an important degree of freedom to study the effect of change in phonon energies while leaving the electronic properties unaffected. This has helped to unravel phenomena such as e.g. the phonon-mediated superconductivity [70].

First, we discuss the inner tube growth from isotope labeled fullerenes [51], and second we present the growth of inner tubes from isotope labeled organic solvents [71].

Commercial ^{13}C isotope enriched fullerenes with two different enrichment grades were used to grow isotope enriched inner tubes. Fullerene encapsulation

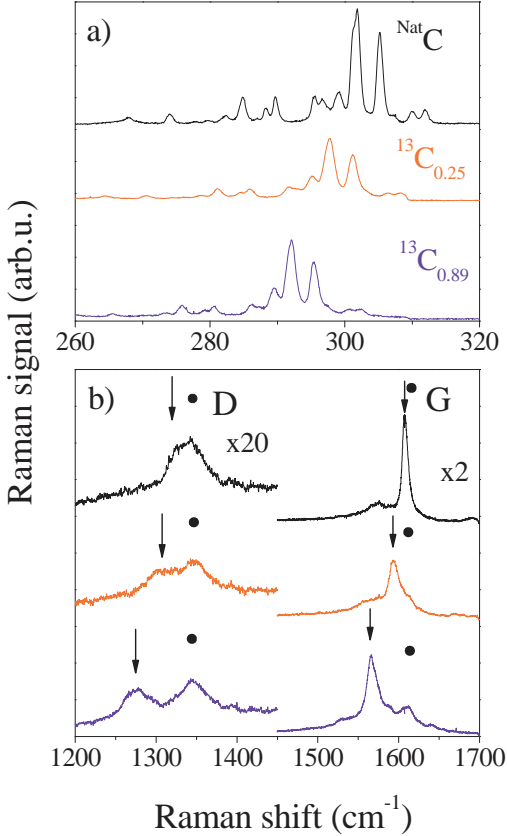


Figure 11: Raman spectra of DWCNTs with natural carbon and ^{13}C enriched inner tubes at 676 nm laser excitation and 90 K. The inner tube RBM (a) and D and G mode spectral ranges (b) are shown. Arrows and filled circles indicate the D (left) and G (right) modes corresponding to the inner and outer tubes, respectively. Reprinted figure with permission from Ref. [51], F. Simon *et al.* Phys. Rev. Lett. **95**, 017401 (2005). Copyright (2005) by the American Physical Society.

[33] and inner tube growth was performed with the conventional methods [35]. This results in a compelling isotope engineered system: double-wall carbon nanotubes with ^{13}C isotope enriched inner walls and outer walls containing natural carbon [51].

In Fig. 11a, we show the inner tube RBM range Raman spectra for a natural DWCNT and two DWCNTs with differently enriched inner walls, 25 % and 89 %. These two latter samples are denoted as $^{13}\text{C}_{25}$ - and $^{13}\text{C}_{89}$ -DWCNT, respectively. The inner wall enrichment is taken from the nominal enrichment of the fullerenes used for the peapod production, whose value is slightly refined based on the Raman data. An overall downshift of the inner tube RBMs is observed for the ^{13}C enriched materials accompanied by a broadening of the lines. The downshift is clear evidence for the effective ^{13}C enrichment of inner tubes. The magnitude of the enrichment and the origin of the broadening are discussed below.

The RBM lines are well separated for inner and outer tubes due to the $\nu_{\text{RBM}} \propto 1/d$ relation and a mean inner tube diameter of $d \sim 0.7$ nm [46, 49]. However, other vibrational modes such as the defect induced D and the tangential G modes strongly overlap for inner and outer tubes. Arrows in Fig. 11b indicate a gradually downshifting component of the observed D and G modes. These components are assigned to the D and G modes of the inner tubes. The sharper appearance of the inner tube G mode, as compared to the response from the outer tubes, is related to the excitation of semiconducting inner tubes and metallic outer tubes [38, 49].

The shifts for the RBM, D and G modes can be analyzed for the two grades of enrichment. The average value of the relative shift for these modes was found to be $(\nu_0 - \nu) / \nu_0 = 0.0109(3)$ and $0.0322(3)$ for the $^{13}\text{C}_{0.25}$ - and $^{13}\text{C}_{0.89}$ -DWCNT samples, respectively. Here, ν_0 and ν are the Raman shifts of the same inner tube mode in the natural carbon and enriched materials, respectively. In the simplest continuum model, the shift originates from the increased mass of the inner tube walls. This gives $(\nu_0 - \nu) / \nu_0 = 1 - \sqrt{\frac{12+c_0}{12+c}}$, where c is the concentration of the ^{13}C enrichment on the inner tube, and $c_0 = 0.011$ is the natural abundance of ^{13}C in carbon. The resulting values of c are 0.277(7) and 0.824(8) for the 25 and 89 % samples, respectively.

The growth of isotope labeled inner tubes allows to address whether carbon exchange between the two walls occurs during the inner tube growth. In Fig.

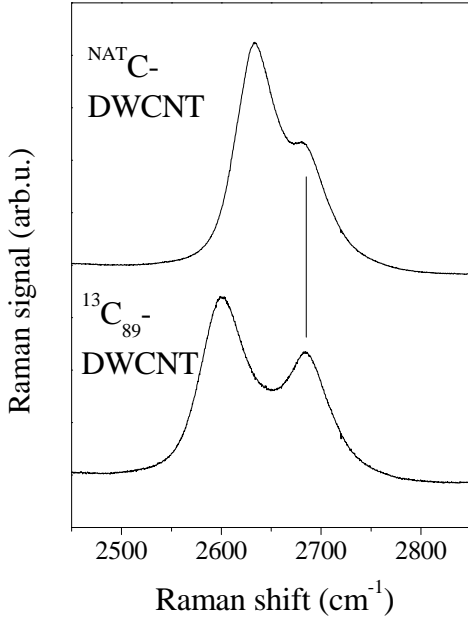


Figure 12: G' spectral range of DWCNTs with natural carbon and ^{13}C enriched inner walls with 515 nm laser excitation. Note the unchanged position of the outer tube G' mode indicated by a vertical line.

12, we show the G' spectral range for DWCNTs with natural carbon and ^{13}C enriched inner walls with 515 nm laser excitation. The G' mode of DWCNTs is discussed in detail in Ref. [57]: the upper G' mode component corresponds to the outer tubes and the lower to the inner tubes. The outer tube G' components are unaffected by the ^{13}C enrichment within the 1 cm^{-1} experimental accuracy. This gives an upper limit to the extra ^{13}C in the outer wall of 1.4 %. This proves that there is no sizeable carbon exchange between the two walls as this would result in a measurable ^{13}C content on the outer wall, too.

The narrow RBMs of inner tubes and the freedom to control their isotope enrichment allows to precisely compare the isotope related phonon energy changes in the experiment and in *ab-initio* calculations. This was performed by J. Kürti and V. Zólyomi in Ref. [51]. The validity of the above sim-

ple continuum model for the RBM frequencies was verified by performing first principles calculations on the $(n, m) = (5, 5)$ tube as an example. In the calculation, the Hessian matrix was determined by DFT using the Vienna Ab Initio Simulation Package [72]. Then, a large number of random ^{13}C distributions were generated and the RBM vibrational frequencies were determined from the diagonalization of the dynamical matrix for each individual distribution. It turns out that the calculation can account for the above mentioned broadening of the RBM lines due to the random distribution of the ^{12}C and ^{13}C nuclei [51].

The known characteristics of isotope labeled inner tubes allow to study the possibility of inner tube growth from non-fullerene carbon sources [71]. For this purpose, we chose organic solvents containing aromatic rings, such as toluene and benzene. These are known to wet the carbon nanotubes and are appropriate solvents for fullerenes. As described in the following, the organic solvents indeed contribute to the inner tube growth, however only in the presence of C_{60} “stopper” molecules [71]. In the absence of co-encapsulated fullerenes the solvents alone give no inner tube.

The fullerene+organic solvents encapsulation was performed by dissolving typically 150 μg fullerenes in 100 μl solvents and then sonicating with 1 mg SWCNT in an Eppendorf tube for 1 h. The weight uptake of the SWCNT is $\sim 15\text{ \%}$ [51] that is shared between the solvent and the fullerenes. The peapod material was separated from the solvent by centrifuging and it was then greased on a sapphire substrate. The solvent prepared peapods were treated in dynamic vacuum at 1250 $^{\circ}\text{C}$ for 2 hours for the inner tube growth. The inner tube growth efficiency was found independent of the speed of warming.

The growth of inner tubes from the solvents can be best proven by the use of C_{60} containing natural carbon and a solvent mixture consisting of ^{13}C enriched and natural carbon containing solvents with varying concentrations. Toluene was a mixture of ring ^{13}C labeled ($^{13}\text{C}_6\text{H}_6\text{-NATCH}_3$) and natural toluene ($\text{NATC}_6\text{H}_5\text{CH}_3$). Benzene was a mixture of ^{13}C enriched and natural benzene. The labeled site was $> 99\text{ \%}$ ^{13}C labeled for both types of molecules. The ^{13}C con-

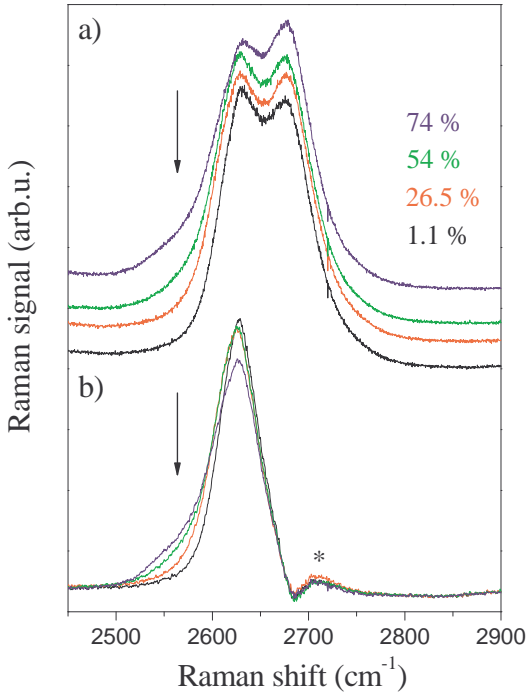


Figure 13: a) The G' mode of toluene+C₆₀ peapod based DWCNTs with varying ¹³C enrichment at 515 nm laser excitation. From top to bottom: 74 %, 54 %, 26.5 % and natural ¹³C content. b) The G' mode of the inner tubes after subtracting the experimental SWCNT spectrum. A small residual peak is observed around 2710 cm⁻¹ (denoted by an asterisk) due to the imperfect subtraction. Arrows indicate the spectral weight shifted toward lower frequencies. Reprinted figure with permission from Ref. [71], F. Simon and H. Kuzmany, Chem. Phys. Lett. **425**, 85 (2006). Copyright (2006) by Elsevier.

tent, x , of the solvent mixtures was calculated from the concentration of the two types of solvents and by taking into account the presence of the naturally enriched methyl-group for the toluene. In Fig. 13a, we show the G' modes of DWCNTs with varying ¹³C labeled content in toluene+C₆₀ based samples and in Fig. 13b, we show the same spectra after subtracting the outer SWCNT component. A shoulder appears for larger values of x on the low frequency side of the inner tube mode, whereas the outer tube mode is unchanged. Similar behavior was observed for the benzene+C₆₀ based peapod samples (spectra not shown) although with a somewhat smaller spectral intensity of the shoulder. The appearance of this low frequency shoulder is evidence for the presence of a sizeable ¹³C content in the inner tubes. This proves that the solvent indeed contributes to the inner tube formation as it is the only sizeable source of ¹³C in the current samples. The appearance of the low frequency shoulder rather than the shift of the full mode indicates an inhomogeneous ¹³C enrichment. A possible explanation is that smaller diameter nanotubes might be higher ¹³C enriched as they retain the solvent better than larger tubes.

To quantify the ¹³C enrichment of the inner tubes, the downshifted spectral weight of the inner tube G' mode was determined from the subtracted spectra in Fig. 14b. The subtraction does not give a flat background above 2685 cm⁻¹, however it is the same for all samples and has a small spectral weight, thus it does not affect the current analysis. The line-shapes strongly deviate from an ideal Lorentzian profile. Therefore the line positions cannot be determined by fitting, whereas the first moments are well defined quantities. The effective ¹³C enrichment of the inner tubes, c , is calculated from $(\nu_0 - \nu) / \nu_0 = 1 - \sqrt{\frac{12+c_0}{12+c}}$, where ν_0 and ν are the first moments of the inner tube G' mode in the natural carbon and enriched materials, respectively, and $c_0 = 0.011$ is the natural abundance of ¹³C in carbon. The validity of this “text-book formula” is discussed above and it was verified by *ab-initio* calculations for enriched inner tubes in Ref. [51]. In Fig. 14, we show the effective ¹³C content in the inner tubes as a function of the ¹³C content in the starting solvents.

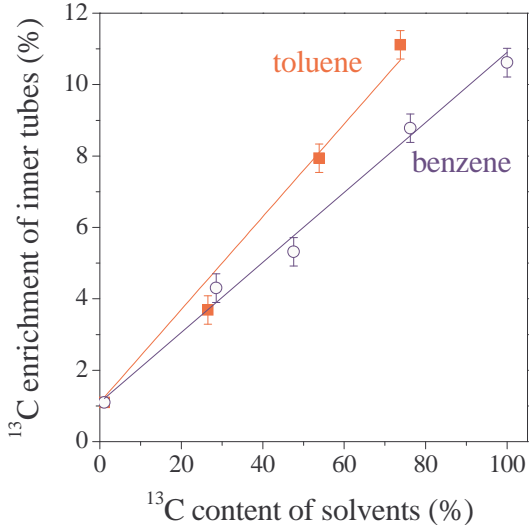


Figure 14: ^{13}C content of inner tubes based on the first moment analysis as explained in the text as a function of ^{13}C enrichment of benzene and toluene. Lines are linear fits to the data and are explained in the text. Reprinted figure with permission from Ref. [71], F. Simon and H. Kuzmany, *Chem. Phys. Lett.* **425**, 85 (2006). Copyright (2006) by Elsevier.

The scaling of the ^{13}C content of the inner tubes with that in the starting solvents proves that the source of the ^{13}C is indeed the solvents. The highest value of the relative shift for the toluene based material, $(\nu_0 - \nu) / \nu_0 = 0.0041(2)$, corresponds to about 11 cm^{-1} shift in the first moment of the inner tube mode. The shift in the radial breathing mode range (around 300 cm^{-1}) [55] would be only 1 cm^{-1} . This underlines why the high energy G' mode is convenient for the observation of the moderate ^{13}C enrichment of the inner tubes. When fit with a linear curve with $c_0 + A * x$, the slope, A directly measures the carbon fraction in the inner tubes that originates from the solvents.

The synthesis of inner tubes from organic solvent proves that any form of carbon that is encapsulated inside SWCNTs contributes to the growth of inner tubes. As mentioned above, inner tubes are not

formed in the absence of fullerenes but whether the fullerene is C_{60} or C_{70} does not play a role. It suggests that fullerenes act only as a stopper to prevent the solvent from evaporating before the synthesis of the inner tube takes place. It also clarifies that the geometry of fullerenes do not play a distinguished role in the inner tube synthesis as it was originally suggested [68, 69]. It also proves that inner tube growth can be achieved irrespective of the carbon source, which opens a new prospective to explore the in-the-tube chemistry with other organic materials.

3.3 ESR studies on encapsulated magnetic fullerenes

Observation of the intrinsic ESR signal of pristine SWCNTs remains elusive [73, 74]. Now, it is generally believed that intrinsic ESR of the tubes can not be observed as conduction electrons on metallic tubes are relaxed by defects too fast to be observable. In addition, one always observes a number of ESR active species in a sample, such as graphitic carbon or magnetic catalyst particles, which prevent a meaningful analysis of the signal. In contrast, local probe studies could still allow an ESR study of tubes, provided the local spin probe can be selectively attached to the tubes. This goal can be achieved by using magnetic fullerenes, such as e.g. $\text{N}@C_{60}$ or C_{59}N , since fullerenes are known to be selectively encapsulated inside SWCNTs [31] and can be washed from the outside using organic solvents [33]. As the properties and handling of the two magnetic fullerenes are quite different, the synthesis of the corresponding peapods and the results are discussed separately.

$\text{N}@C_{60}$ is an air stable fullerene [75] but decays rapidly above $\sim 200 \text{ }^\circ\text{C}$ [76] which prevents the use of the conventional vapor method of peapod preparation which requires temperatures above $400 \text{ }^\circ\text{C}$. To overcome this limitation and to allow in general the synthesis of temperature sensitive peapod materials, low temperature peapod synthesis (solvent method) was developed independently by four groups [39, 40, 41, 42]. These methods share the common idea of mixing the opened SWCNTs with C_{60} in a solvent with low fullerene solubility such as methanol [39] or n-pentane [40]. The encapsu-

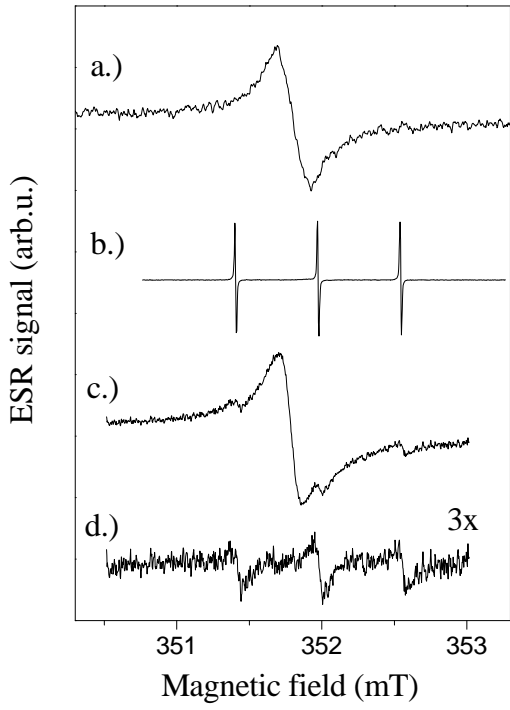


Figure 15: X-band electron spin resonance spectrum of the a.) pristine SWCNT, b.) crystalline $\text{N@C}_{60}:\text{C}_{60}$, c.) $(\text{N@C}_{60}:\text{C}_{60})@\text{SWCNT}$ and d.) the triplet component of the $(\text{N@C}_{60}:\text{C}_{60})@\text{SWCNT}$ ESR spectrum at ambient temperature. Reprinted figure with permission from Ref. [40], F. Simon *et al.* *Chem. Phys. Lett.* **383**, 362 (2004). Copyright (2004) by Elsevier.

lation is efficient as it is energetically preferred for C_{60} to enter the tubes rather than staying in the solution. After the solvent filling, excess fullerenes can be removed by sonication in toluene, which is a good fullerene solvent as it was found that fullerenes enter the tube irreversibly. HR-TEM has shown an abundant filling with the fullerenes [39, 41] and a more macroscopic characterization using Raman spectroscopy has proven that peapods prepared by the solvent method are equivalent to the vapor prepared peapods [40].

The low temperature synthesis allows to encapsulate the N@C_{60} fullerene. The $\text{N@C}_{60}:\text{C}_{60}$ endohedral fullerene: fullerene solid solution can be produced in a N_2 arc-discharge tube following Ref. [77] with a typical yield of a few 10 ppm [78]. In Fig. 15., the ESR spectra of the starting SWCNT, $(\text{N@C}_{60}:\text{C}_{60})@\text{SWCNT}$, and $\text{N@C}_{60}:\text{C}_{60}$ are shown. The ESR spectrum of the pristine SWCNT for the magnetic field range shown is dominated by a signal that is assigned to some residual carbonaceous material, probably graphite. Fig. 15c. shows, that after the solvent encapsulation of $\text{N@C}_{60}:\text{C}_{60}$ in the NCL-SWCNT, a hyperfine N triplet ESR is observed, similar to that in pristine $\text{N@C}_{60}:\text{C}_{60}$, superimposed on the broad signal present in the pristine nanotube material. Fig. 15d. shows the triplet component of this signal after subtracting the signal observed in pristine SWCNT. The hyperfine triplet in $\text{N@C}_{60}:\text{C}_{60}$ is the result of the overlap of the ${}^4\text{S}_{3/2}$ state of the three 2p electrons of the N atom and the ${}^{14}\text{N}$ nucleus, with nuclear spin, $I = 1$. The isotropic hyperfine coupling of $\text{N@C}_{60}:\text{C}_{60}$ is unusually high as a result of the strongly compressed N atomic 2p³ orbitals in the C_{60} cage thus it unambiguously identifies this material [75]. The hyperfine coupling constant observed for the triplet structure in the encapsulated material, $A_{\text{iso}} = 0.57 \pm 0.01$ mT, agrees within experimental precision with that observed in $\text{N@C}_{60}:\text{C}_{60}$ [75], which proves that the encapsulated material is $(\text{N@C}_{60}:\text{C}_{60})@\text{SWCNT}$. The ESR linewidth for the encapsulated material, $\Delta H_{pp} = 0.07$ mT, is significantly larger than the resolution limited $\Delta H_{pp} = 0.01$ mT in the pristine $\text{N@C}_{60}:\text{C}_{60}$ material, the lines being Lorentzian. The most probable cause for the broadening is static magnetic fields from residual magnetic impurities in the SWCNT [79]. The ESR signal intensity is proportional to the number of N spins, and this allows the quantitative comparison of N concentrations in $(\text{N@C}_{60}:\text{C}_{60})@\text{SWCNT}$ and $\text{N@C}_{60}:\text{C}_{60}$. It was found that the number of observed N@C_{60} spins is consistent with the number expected from a good filling efficiency [40].

As seen from the ESR results on encapsulated N@C_{60} , relatively limited information can be deduced about the tubes themselves. This stems from the fact that the N spins are well shielded in N@C_{60}

[80] and are thus are relatively insensitive to the SWCNT properties. In contrast, N@C_{60} @SWCNT peapods might find another application as building elements of a quantum computer as proposed by Harneit *et al.* [8]. A better candidate for magnetic fullerene encapsulation is the C_{59}N monomer radical as here the unpaired electron is on the cage and is a sensitive probe of the environment. This material can be chemically prepared [81], however it forms a non-magnetic dimer crystal (C_{59}N)₂. It appears as a spinless monomer in an adduct form [82] or attached to surface dangling bonds [83]. The magnetic C_{59}N monomer radical is air sensitive but it can be stabilized as a radical when it is dilutely mixed in C_{60} [84]. As a result, a different strategy has to be followed to encapsulate C_{59}N inside SWCNT, which is discussed in the following along with preliminary ESR results [85].

To obtain C_{59}N peapods, air stable C_{59}N derivatives, (C_{59}N -der in the following) were prepared chemically by A. Hirsch and F. Hauke following standard synthesis routes [82, 86]. The C_{59}N -der was 4-Hydroxy-3,5-dimethyl-phenyl-hydroazafullerene. The C_{59}N derivatives were encapsulated either pure or mixed with C_{60} as C_{59}N -der: C_{60} with 1:9 concentrations using a modified version of the low temperature encapsulation method. In brief, the mixture of the dissolved fullerenes and SWCNTs were sonicated in toluene and filtered. It is expected that the C_{59}N monomer radical can be obtained after a heat treatment in dynamic vacuum, which is discussed below.

Raman spectroscopy was performed to characterize the SWCNT filling with the C_{59}N -der [85]. The major Raman modes of the pristine C_{59}N -der are similar to those of the (C_{59}N)₂ dimer [87]. The strongest mode is observed at 1459.2 cm^{-1} which is derived from the C_{60} $A_g(2)$ mode and is downshifted to 1457 cm^{-1} after the encapsulation procedure. The 2.2 cm^{-1} downshift proves the encapsulation of the molecule inside the SWCNT. When encapsulated inside SWCNTs, the corresponding $A_g(2)$ mode of C_{60} downshifts with 3 cm^{-1} , which is assigned to the softening of the C_{60} $A_g(2)$ vibrational mode due to the interaction between the ball and the SWCNT wall [43].

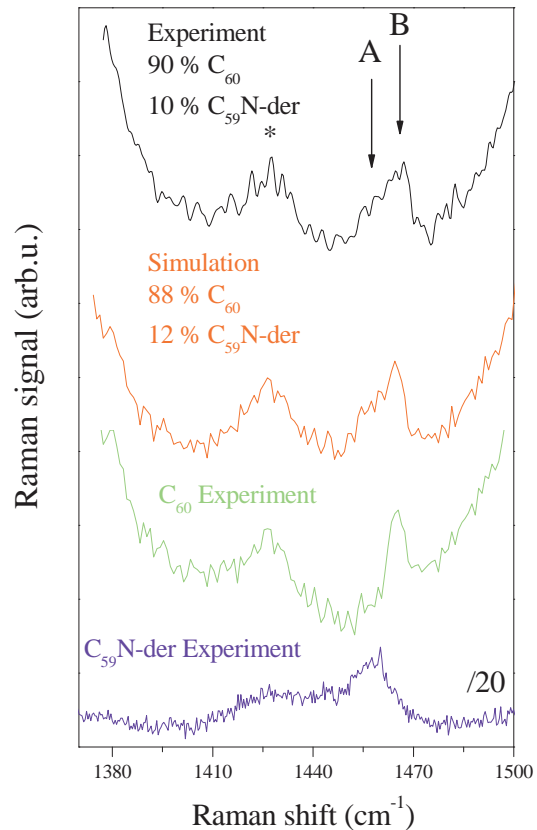


Figure 16: Raman spectra of the encapsulated C_{59}N -der: C_{60} mixture at the 488 nm laser excitation. The spectra for the C_{59}N -der and C_{60} peapods is shown together with their weighted sum as explained in the text. A and B mark the components coming nominally from the superposing two phases. The asterisk marks a mode that is present in the pristine SWCNT material. Note the different scale for the C_{59}N -der peapod material. Reprinted figure with permission from Ref. [85], F. Simon *et al.* Carbon, **44**, 1958 (2006). Copyright (2006) by Elsevier.

The integrated intensity of the observed $A_g(2)$ derived mode of the $C_{59}N$ is approximately 5 times larger than that of a C_{60} peapod prepared identically when normalized by the SWCNT G mode intensity. This, however, can not be used to measure the encapsulation efficiency as Raman intensities depend on the strength of the Raman resonance enhancement and the Raman scattering matrix elements [50]. For C_{60} peapods the Raman signal was calibrated with independent and carbon number sensitive measurements: EELS studies gave the total number of C_{60} related and non- C_{60} related carbons [66] and the mass of encapsulated C_{60} s was determined from NMR studies using ^{13}C enriched fullerenes [51, 88]. In the current case, neither methods can be employed and we determined the filling efficiency for the azafullerene by encapsulating a mixture of the azafullerene and C_{60} . In Fig. 16, the Raman spectra of the encapsulated $C_{59}N$ -der: C_{60} mixture with weight ratios of 1:9 in the starting solvent is shown. The Raman spectrum of the encapsulated mixture was simulated with a weighted sum of the separately recorded spectra for encapsulated $C_{59}N$ -der and C_{60} . The best agreement between the simulated and the experimental spectra is for a $C_{59}N$ -der content of 0.12(2). This value is close to the expected value of 0.1 and it proves that the azafullerene enters the tubes with the same efficiency as C_{60} .

Fig. 17 shows the room temperature ESR spectra of $C_{59}N:C_{60}$ @SWCNT after 600 °C vacuum annealing from Ref. [89]. The spectra of $C_{59}N:C_{60}$, a $C_{59}N$ monomer embedded in C_{60} [84], is also shown for comparison. This latter spectrum was previously assigned to the superposition of rotating $C_{59}N$ monomers and bound $C_{59}N-C_{60}$ heterodimers [90]. The large spin density at the ^{14}N nucleus of the rotating $C_{59}N$ molecule results in an ESR triplet signal and the $C_{59}N-C_{60}$ heterodimer has a singlet signal (arrow in Fig. 17) as the spin density resides on the C_{60} molecule. ^{14}N triplet structures are observed in the peapod samples with identical hyperfine coupling as in the crystalline sample and are thus identified as the ESR signals of rotating $C_{59}N$ monomer radicals encapsulated inside SWCNTs. The additional component (arrow in Fig. 17) observed for sample B, which contains co-encapsulated C_{60} , is iden-

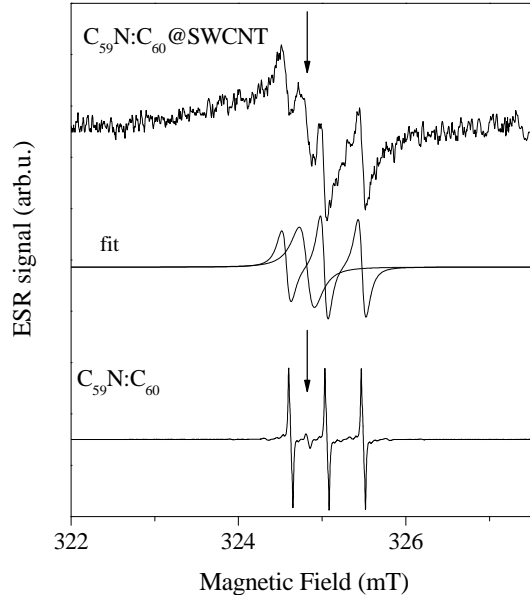


Figure 17: ESR spectra of crystalline $C_{59}N:C_{60}$ (a) and $(C_{59}N:C_{60})@SWCNT$ obtained by annealing the $(C_{59}N\text{-der}:C_{60})@SWCNT$. Solid curves show the deconvolution of the different ESR components for the encapsulated material. Reprinted figure with permission from Ref. [51], F. Simon *et al.* Phys. Rev. Lett. **97**, 136801 (2006). Copyright (2006) by the American Physical Society.

tified as $C_{59}N-C_{60}$ heterodimers encapsulated inside SWCNTs since this signal has the same g -factor as in the crystalline material. This singlet line is absent in sample A which does not contain C_{60} . For both peapod samples a broader line with HWHM of $\Delta H \sim 0.6$ mT is also observed. The broader component appears also on heat treatment of reference samples without encapsulated $C_{59}N$ -der and is identified as a side-product. Annealing at 600 °C is optimal: lower temperatures result in smaller $C_{59}N$ signals and higher temperatures increase the broad impurity signal without increasing the $C_{59}N$ intensity.

The observation of the ESR signal of $C_{59}N$ related spins proves that after the 600 °C heat treatment, a sizeable amount of rotating $C_{59}N$ monomer radi-

cals are present in the sample. This is not surprising in the view of the ability to form $C_{59}N$ monomers from $C_{59}N$ at similar temperatures [91], however the current process is not reversible and the remnants of the side-groups are probably removed by the dynamic pumping.

3.4 NMR studies on isotope engineered heteronuclear nanotubes

The growth of the “isotope engineered” nanotubes, i.e. DWCNTs with highly enriched inner wall allows to study the electronic properties of small diameter carbon nanotubes with an unprecedented specificity using NMR. For normal SWCNTs, either grown from natural or ^{13}C enriched carbon, the NMR signal originates from all kinds of carbon like amorphous or graphitic carbon.

NMR allows to determine the macroscopic amount of enriched tubes as it is sensitive to the number of ^{13}C nuclei in the sample. In Fig. 18, we show the static and magic angle spinning spectra of ^{13}C enriched DWCNTs, and the static spectrum for the SWCNT material. The mass fraction which belongs to the highly enriched phase can be calculated from the integrated signal intensity by comparing it to the signal intensity of the 89 % ^{13}C enriched fullerene material. It was found that the mass fraction of the highly enriched phase relative to the total sample mass is 13(4) % which agrees with the expected value of 15 %. The latter is obtained from the SWCNT purity (50 %), ~ 70 % volume filling for peapod samples [66], and the mass ratio of encapsulated fullerenes to the mass of the SWCNTs. This suggests that the NMR signal comes nominally from the inner tubes, and other carbon phases such as amorphous or graphitic carbon are non ^{13}C enriched.

The typical chemical shift anisotropy (CSA) powder pattern was observed for the SWCNT sample in agreement with previous reports [79, 92]. However, the static DWCNT spectrum cannot be explained with a simple CSA powder pattern even if the spectrum is dominated by the inner tube signal. The complicated structure of the spectrum suggests that the chemical shift tensor parameters are highly distributed for the inner tubes. It is the result of the

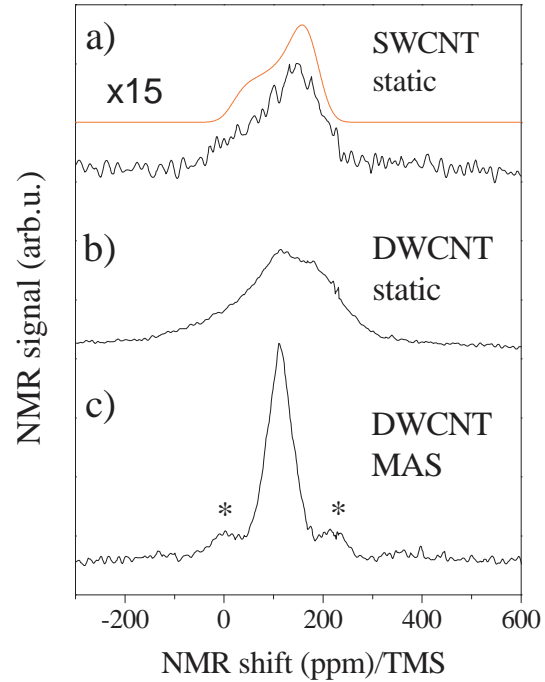


Figure 18: NMR spectra normalized by the total sample mass, taken with respect to the tetramethylsilane (TMS) shift. (a) Static spectrum for non-enriched SWCNT enlarged by 15. Smooth solid line is a chemical shift anisotropy powder pattern simulation with parameters published in the literature [79]. (b) Static and (c) MAS spectra of $^{13}C_{0.89}$ -DWCNT, respectively. Asterisks show the sidebands at the 8 kHz spinning frequency. Reprinted figure with permission from Ref. [51], F. Simon *et al.* Phys. Rev. Lett. **95**, 017401 (2005). Copyright (2005) by the American Physical Society.

higher curvature of inner tubes as compared to the outer ones: the variance of the diameter distribution is the same for the inner and outer tubes [93] but the corresponding bonding angles show a larger variation [94]. In addition, the residual line-width in the MAS experiment, which is a measure of the sample inhomogeneity, is 60(3) ppm, i.e. about twice as large as the \sim 35 ppm found previously for SWCNT samples [79, 92]. The isotropic line position, determined from the MAS measurement, is 111(2) ppm. This value is significantly smaller than the isotropic shift of the SWCNT samples of 125 ppm [79, 92]. However, recent theoretical *ab-initio* calculations by F. Mauri and co-workers have successfully explained this anomalous isotropic chemical shift [95]. It was found that diamagnetic demagnetizing currents on the outer walls cause the diamagnetic shift of the inner tube NMR signal.

In addition to the line position, dynamics of the nuclear relaxation is a sensitive probe of the local electronic properties [96]. The electronic properties of the nanotubes was probed using the spin lattice relaxation time, T_1 , defined as the characteristic time it takes the ^{13}C nuclear magnetization to recover after saturation [88]. The signal intensity after saturation, $S(t)$, was deduced by integrating the fast Fourier transform of half the spin-echo for different delay times t . The data were taken with excitation pulse lengths $\pi/2 = 3.0 \mu\text{s}$ and short pulse separation times of $\tau = 15 \mu\text{s}$ [96]. The value of T_1 was obtained by fitting the t dependence of $S(t)$ to the form $S(t) = S_a - S_b \cdot M(t)$, where $S_a \simeq S_b (> 0)$ are arbitrary signal amplitudes, and

$$M(t) = \exp \left[-(t/T_1^e)^\beta \right], \quad (2)$$

is the reduced magnetization recovery of the ^{13}C nuclear spins. It was found that $M(t)$ does not follow the single exponential form with $\beta = 1$, but instead fits well to a stretched exponential form with $\beta \simeq 0.65(5)$, implying a distribution in the relaxation times T_1 . For a broad range of experimental conditions, the upper 90 % of the $M(t)$ data is consistent with constant $\beta \simeq 0.65(5)$, implying a field and temperature independent underlying distribution in T_1 .

The collapse of the data with constant $\beta = 0.65(5)$ is a remarkable experimental observation and it implies that each inner-tube in the powder sample has a different value of T_1 , yet *all* the T_1 components and therefore all the inner-tubes follow the same T and H dependence within experimental uncertainty. This finding is in contrast to earlier reports in SWCNTs where $M(t)$ fits well to a bi-exponential distribution, 1/3 of which had a short T_1 value characteristic of fast relaxation from metallic tubes, and the remaining 2/3 had long T_1 corresponding to the semiconducting tubes [79, 92, 97, 98], as expected from a macroscopic sample of SWCNTs with random chiralities.

The bulk average T_1^e defined in Eq. (2) can be considered and its uniform T and H dependence can be followed. The $M(t)$ data can be fitted with the constant exponent $\beta = 0.65(5)$, which reduces unnecessary experimental scattering in T_1^e . In Fig. 19, we show the temperature dependence of $1/T_1^e T$ for two different values of the external magnetic field, H . The data can be separated into two temperature regimes; the high temperature regime $\gtrsim 150 \text{ K}$, and the low T regime $\lesssim 150 \text{ K}$. At high temperatures, $1/T_1^e T$ is independent of T which indicates a metallic state [96] for all of the inner tubes. A strong magnetic field dependence for T_1 was also observed, which was explained by a 1D spin diffusion mechanism for T_1 [88].

The experimentally observed uniform metallicity of inner tubes is a surprising observation. This was suggested to be caused by the shifting of the inner tube Fermi levels due to charge transfer between the two tube walls. Indeed, using *ab-initio* calculations Okada and Oshiyama have found that DWCNTs made of non-metallic zig-zag inner-outer tubes, such as the (7,0)@(16,0) DWCNT, are metallic [99]. The direction of the charge transfer goes against the Faraday effect as inner tubes are electron and outer tubes are hole doped. Although, calculations are difficult if not impossible for an arbitrary inner-outer tube pair, this result confirms that two non-metallic tubes when producing an inner tube can render the electronic structure metallic.

The origin of the unusual T dependence of $1/T_1^e T$ in the low temperature regime ($\lesssim 150 \text{ K}$) is pecu-

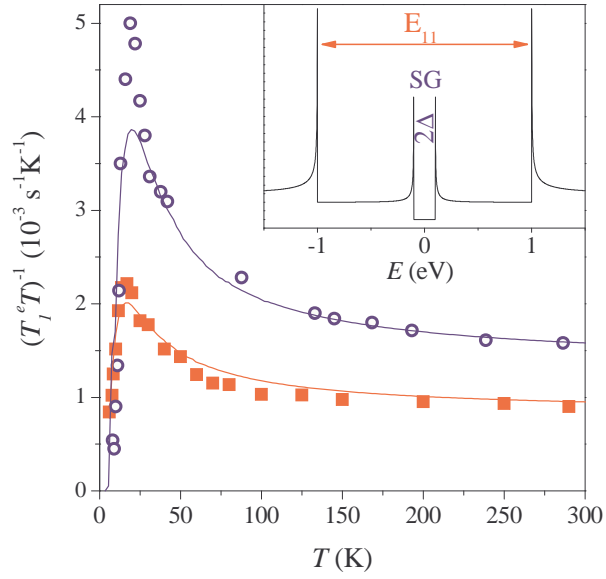


Figure 19: Temperature dependence of spin-lattice relaxation rate divided by temperature, $1/T_1^e T$, in units of $(10^3 \times s^{-1} K^{-1})$ for 3.6 T (○) and 9.3 T (■). Grey curves are best fits to Eq. (4) with $2\Delta = 46.8(40.2)$ K for $H = 3.6(9.3)$ Tesla, respectively. Inset shows the suggested DOS with a small energy, 2Δ secondary gap at the Fermi level of metallic inner tubes, which is displayed not to scale. Note the van Hove singularities (vHs) at $\pm\Delta$. Reprinted figure with permission from Ref. [88], P. M. Singer *et al.* Phys. Rev. Lett. **95**, 236403 (2005). Copyright (2005) by the American Physical Society.

liar. Some explanations can be ruled out as its origin. Firstly, one can rule out the possibility of an activation type mechanism where T_1 is dominated by fluctuating hyperfine fields with a characteristic time scale τ which increases with decreasing T (i.e. glassy slowing). This would result in a peaked relaxation with a strongly field dependent peak value [96], which is clearly not the case. Furthermore at low T , $1/T_1^e T$ drops below its high temperature value, which rules out the possibility of a T independent component in $1/T_1^e T$ plus an activated component on top. Secondly, the possibility of a simple $1/T$ Curie-like T dependence in $1/T_1^e T$ as a result of paramagnetic centers in the sample can be ruled out. This can be inferred from the pronounced gap in $1/T_1^e T$, together with the fact that no loss of ^{13}C NMR signal intensity in the entire temperature range of the experiment was observed.

The simplest possible explanation for the experimental data is a non-interacting electron model of a 1D semiconductor with a small secondary gap (SG). The $1/T_1^e T$ data can be fitted using this model with only one parameter, the homogeneous SG, 2Δ . The normalized form of the gapped 1D density-of-states $n(E)$

$$n(E) = \begin{cases} \frac{E}{\sqrt{E^2 - \Delta^2}} & \text{for } |E| > \Delta \\ 0 & \text{otherwise} \end{cases} \quad (3)$$

here, E is taken with respect to the Fermi energy). The total DOS of an inner tube is shown schematically in the insert of Fig. 19. Eq. (3) is used to calculate $1/T_1^e T$ [100] as such

$$\frac{1}{T_1^e T} = \alpha(\omega) \int_{-\infty}^{\infty} n(E) n(E + \omega) \left(-\frac{\delta f}{\delta E} \right) dE, \quad (4)$$

where E and ω are in temperature units for clarity, f is the Fermi function $f = [\exp(E/T) + 1]^{-1}$, and the amplitude factor $\alpha(\omega)$ is the high temperature value for $1/T_1^e T$. The results of the best fit of the data to Eq. (4) are presented in Fig. 19, where $2\Delta = 43(3)$ K ($\equiv 3.7$ meV) is H independent within experimental scattering between 9.3 and 3.6 Tesla.

The origin of the experimentally observed gap still remains to be clarified. Tight binding calcula-

tions predict that applied magnetic fields can induce SG's of similar magnitude for metallic SWCNT [101]. However, such a scenario can be excluded due to the absence of any field dependence of the gap. The NMR data would be more consistent with a curvature induced SG for metallic tubes [9, 102, 103, 47], however for the typical inner-tubes the predicted values, ~ 100 meV, are over an order of magnitude larger than our experimental data. Other scenarios, such as quantization of levels due to finite short lengths of the nanotubes could be considered as well, however, in all these cases a behavior independent of tube size and chirality is certainly not expected.

This suggests that electron-electron interactions may play an important role for the metallic inner tubes. It has been predicted that electron-electron correlations and a Tomonaga-Luttinger (TLL) state leads to an increase in $1/T_1T$ with decreasing T [104], which is a direct consequence of the 1D electronic state. The correlated 1D nature may also lead to a Peierls instability [10] with the opening of a small collective gap 2Δ and a sharp drop in $1/T_1T$ below $\Delta \sim 20$ K. Therefore, the presence of both a TLL state and a Peierls instability could possibly account for the data.

Summarizing the NMR studies, it was shown that T_1 has a similar T and H dependence for all the inner-tubes, with no indication of a metallic/semiconducting separation due to chirality distribution. At high temperatures, ($T \gtrsim 150$ K) $1/T_1^eT$ of the inner tubes exhibit a metallic 1D spin diffusion state. Below ~ 150 K, $1/T_1^eT$ increases dramatically with decreasing T , and a gap in the spin excitation spectrum is found below $\Delta \simeq 20$ K, which is suggested to be caused by a Peierls instability [10, 55].

4 Summary

In summary, we reviewed how in-the-tube functionalization of SWCNTs can be used to study various properties of the tubes themselves. Inner tubes grown from encapsulated fullerenes were shown to be an excellent probe of diameter dependent reactions on the outer tubes. Inner tubes grown from isotope labeled fullerenes and organic solvents allowed to understand

the role of the different carbon phases in the growth of the inner tubes. In addition, isotope labeled inner tubes were shown to yield an unparalleled precision to study the density of states near the Fermi level using NMR. It was reviewed how magnetic fullerenes can be encapsulated inside SWCNTs yielding linear spin chains with sizeable spin concentrations and also to allow ESR studies of the tube properties.

5 Acknowledgements

This work was supported by the Austrian Science Funds (FWF) project Nr. 17345, by the Hungarian State Grants No. TS049881, F61733 and NK60984, by the EU projects BIN2-2001-00580 and MERG-CT-2005-022103, by the Zoltán Magyary and Bolyai postdoctoral fellowships. J. Bernardi and Ch. Schaman are acknowledged for the HR-TEM contribution and for preparing some of the figures, respectively.

[†]Present address: Budapest University of Technology and Economics, Institute of Physics and Solids in Magnetic Fields Research Group of the Hungarian Academy of Sciences, H-1521, Budapest P.O.Box 91, Hungary

References

- [1] Sumio Iijima. Helical microtubules of graphitic carbon. *Nature*, 354:56–58, 1991.
- [2] Sumio Iijima and Toshinari Ichihashi. Single-shell carbon nanotubes of 1-nm diameter. *Nature*, 363:603–605, 1993.
- [3] D. S. Bethune, C. H. Kiang, M. S. DeVries, G. Gorman, Savoy R., and R. Beyers. Cobalt-catalysed growth of carbon nanotubes with single-atomic-layer walls. *Nature*, 363:605, 1993.
- [4] A. N. Obraztsov, I. Pavlovsky, A. P. Volkov, E. D. Obraztsova, A. L. Chuvilin, and V. L. Kuznetsov. *J. Vac. Sci. Techn. B*, 18:1059, 2000.

[5] G. Z. Yue, Q. Qiu, B. Gao, Y. Cheng, J. Zhang, H. Shimoda, S. Chang, J. P. Lu, and O. Zhou. Generation of continuous and pulsed diagnostic imaging x-ray radiation using a carbon-nanotube-based field-emission cathode. *Appl. Phys. Lett.*, 81:355–368, 2002.

[6] J. H. Hafner, C. L. Cheung, and C. M. Lieber. Growth of nanotubes for probe microscopy tips. *Nature*, 398:761, 1999.

[7] Adrian Bachtold, Peter Hadley, Takeshi Nakanishi, and Cees Dekker. Logic circuits with carbon nanotube transistors. *Science*, 294:1317–1320, 2001.

[8] W. Harneit, C. Meyer, A. Weidinger, D. Suter, and J. Twamley. *Phys. St. Solidi B*, 233:453, 2002.

[9] N. Hamada, S. Sawada, and A. Oshiyama. New one-dimensional conductors: Graphitic microtubules. *Phys. Rev. Lett.*, 68:1579.1581, 1992.

[10] R. Saito, G. Dresselhaus, and M.S. Dresselhaus. *Physical Properties of Carbon Nanotubes*. Imperial College Press, 1998.

[11] D. Chattopadhyay, L. Galeska, and F. Papadimitrakopoulos. A route for bulk separation of semiconducting from metallic single-wall carbon nanotubes. *J. Am. Chem. Soc.*, 125:3370–3375, 2003.

[12] R. Krupke, F. Hennrich, H. von Lohneysen, and M. M. Kappes. Separation of Metallic from Semiconducting Single-Walled Carbon Nanotubes. *Science*, 301:344–347, 2003.

[13] Z. H. Chen, X. Du, M. H. Du, C. D. Rancken, H. P. Cheng, and A. G. Rinzler. *Nano Lett.*, 3:1245–1259, 2003.

[14] M. Zheng, A. Jagota, M. S. Strano, A. P. Santos, P. Barone, S. G. Chou, G Diner, M. S. B. A. Dresselhaus, R. S. McLean, G. B. Onoa, G. G. Samsonidze, E. D. Semke, M. Usrey, and D. J. Walls. 2003. *Science*, 302:1545–1548, 2003.

[15] Sergei M. Bachilo, Michael S. Strano, Carter Kittrell, Robert H. Hauge, Richard E. Smalley, and R. Bruce Weisman. Structure-Assigned Optical Spectra of Single-Walled Carbon Nanotubes. *Science*, 298:2361–2366, 2002.

[16] C. Fantini, A. Jorio, M. Souza, M. S. Strano, M. S. Dresselhaus, and M. A. Pimenta. Optical Transition Energies for Carbon Nanotubes from Resonant Raman Spectroscopy: Environment and Temperature Effects. *Phys. Rev. Lett.*, 93:147406, 2004.

[17] H. Telg, J. Maultzsch, S. Reich, F. Hennrich, and C. Thomsen. Chirality Distribution and Transition Energies of Carbon Nanotubes. *Phys. Rev. Lett.*, 93:177401, 2004.

[18] R. Egger and A. O. Gogolin. Effective low-energy theory for correlated carbon nanotubes. *Nature*, 79:50825085, 1997.

[19] K. P. Bohnen, R. Heid, H. J. Liu, and C. T. Chan. Lattice Dynamics and Electron-Phonon Interaction in (3,3) Carbon Nanotubes. *Phys. Rev. Lett.*, 93:245501–1–4, 2004.

[20] D. Connétable, G.-M. Rignanese, J.-C. Charlier, and X. Blase. Room Temperature Peierls Distortion in Small Diameter Nanotubes. *Phys. Rev. Lett.*, 94:015503–1–4, 2005.

[21] Sander J. Tans, Michel H. Devoret, Hongjie Dai, Andreas Thess, Richard E. Smalley, L. J. Geerligs, and Cees Dekker. Individual single-wall carbon nanotubes as quantum wires. *Nature*, 386:474 – 477, 1997.

[22] C.L. Kane and E.J. Mele. Ratio Problem in Single Carbon Nanotube Fluorescence Spectroscopy. *Phys. Rev. Lett.*, 90:207401–1–4, 2003.

[23] Catalin D. Spataru, Sohrab Ismail-Beigi, Lorin X. Benedict, and Steven G. Louie. Excitonic Effects and Optical Spectra of Single-Walled Carbon Nanotubes. *Phys. Rev. Lett.*, 92:077402–1–4, 2004.

[24] Vasili Perebeinos, J. Tersoff, and Phaedon Avouris. Scaling of Excitons in Carbon Nanotubes. *Phys. Phys. Lett.*, 92:257402–1–4, 2004.

[25] Vasili Perebeinos, J. Tersoff, and Phaedon Avouris. Effect of Exciton-Phonon Coupling in the Calculated Optical Absorption of Carbon Nanotubes. *Phys. Phys. Lett.*, 94:027402–1–4, 2005.

[26] M. Bockrath, D. H. Cobden, Jia Lu, Rinzel A. G., R. E. Smalley, L. Balents, and P. L. McEuen. Luttinger-liquid behaviour in carbon nanotubes. *Nature*, 397:598 – 601, 1999.

[27] H. Ishii, H. Kataura, H. Shiozawa, H. Yoshioka, H. Otsubo, Y. Takayama, T. Miyahara, S. Suzuki, Y. Achiba, M. Nakatake, T. Narimura, M. Higashiguchi, K. Shimada, H. Namatame, and M. Taniguchi. Direct observation of Tomonaga-Luttinger-liquid state in carbon nanotubes at low temperatures. *Nature*, 426:540–544, 2003.

[28] H. Rauf, T. Pichler, M. Knupfer, J. Fink, and H. Kataura. Transition from a Tomonaga-Luttinger Liquid to a Fermi Liquid in Potassium-Intercalated Bundles of Single-Wall Carbon Nanotubes. *Phys. Rev. Lett.*, 93:096805–1–4, 2004.

[29] Feng Wang, Gordana Dukovic, , Louis E. Brus, and Tony F. Heinz. The Optical Resonances in Carbon Nanotubes Arise from Excitons. *Science*, 308:838–841, 2005.

[30] J. Maultzsch, R. Pomraenke, S. Reich, E. Chang, D. Prezzi, A. Ruini, E. Molinari, M. S. Strano, C. Thomsen, and C. Lienau. Exciton binding energies in carbon nanotubes from two-photon photoluminescence. *Phys. Rev. B*, 72:241402, 2005.

[31] Brian W. Smith, Marc Monthioux, and David E. Luzzi. Encapsulated C_{60} in carbon nanotubes. *Nature*, 396:323–324, 1998.

[32] B. W. Smith, M. Monthioux, and D.E. Luzzi. Carbon nanotube encapsulated fullerenes: a unique class of hybrid materials. *Chem. Phys. Lett.*, 315:31–36, 1999.

[33] H. Kataura, Y. Maniwa, T. Kodama, K. Kikuchi, K. Hirahara, K. Suenaga, S. Iijima, S. Suzuki, Y. Achiba, and W. Krätschmer. High-yield fullerene encapsulation in single-wall carbon nanotubes . *Synthetic Met.*, 121:1195–1196, 2001.

[34] B. W. Smith and D.E. Luzzi. Formation mechanism of fullerene peapods and coaxial tubes: a path to large scale synthesis. *Chem. Phys. Lett.*, 321:169–174, 2000.

[35] S. Bandow, M. Takizawa, K. Hirahara, M. Yudasaka, and S. Iijima. Raman scattering study of double-wall carbon nanotubes derived from the chains of fullerenes in single-wall carbon nanotubes. *Chem. Phys. Lett.*, 337:48–54, 2001.

[36] J. L. Hutchison, N. A. Kiselev, E. P. Krinichnaya, A. V. Krestinin, R. O. Loutfy, A. P. Morawsky, V. E. Muradyan, E. D. Obraztsova, J. Sloan, S. V. Terekhov, and D. N. Zakharov. Double-walled carbon nanotubes fabricated by a hydrogen arc discharge method. *Carbon*, 39:761–770, 2001.

[37] Wencai Ren, Feng Li, Jian Chen, Shuo Bai, and Hui-Ming Cheng. Morphology, diameter distribution and Raman scattering measurements of double-walled carbon nanotubes synthesized by catalytic decomposition of methane. *Chem. Phys. Lett.*, 359:196–202, 2002.

[38] R. Pfeiffer, H. Kuzmany, Ch. Kramberger, Ch. Schaman, T. Pichler, H. Kataura, Y. Achiba, J. Kürti, and V. Zólyomi. Unusual High Degree of Unperturbed Environment in the Interior of Single-Wall Carbon Nanotubes. *Phys. Rev. Lett.*, 90:225501–1–4, 2003.

[39] M. Yudasaka, K. Ajima, K. Suenaga, T. Ichihashi, A. Hashimoto, and S. Iijima. Nano-extraction and nano-condensation for C_{60} incorporation into single-wall carbon nanotubes in liquid phases. *Chem. Phys. Lett.*, 380:42–46, 2003.

[40] F. Simon, H. Kuzmany, H. Rauf, T. Pichler, J. Bernardi, H. Peterlik, L. Korecz, F. Fülöp, and A. Jánossy. Low temperature fullerene encapsulation in single wall carbon nanotubes: synthesis of N@C₆₀@SWCNT. *Chem. Phys. Lett.*, 383:362–367, 2004.

[41] M. Monthioux and L. Noé. Room temperature synthesis of C₆₀@SWNT (peapods). In *XVI-IIth International Winterschool on Electronic Properties of Novel Materials.*, 2004. AIP Proceedings.

[42] A. N. Khlobystov, D. A. Britz, J. W. Wang, S. A. O’Neil, M. Poliakoff, and G. A. D. Briggs. Low temperature assembly of fullerene arrays in single-walled carbon nanotubes using supercritical fluids. *J. Mat. Chem.*, 14:2852–2857, 2004.

[43] T. Pichler, H. Kuzmany, H. Kataura, and Y. Achiba. Metallic Polymers of C₆₀ Inside Single-Walled Carbon Nanotubes. *Phys. Rev. Lett.*, 87:267401–1–4, 2001.

[44] F. Simon, Á Kukovecz, Z. Kónya, R. Pfeiffer, and H. Kuzmany. Highly defect-free inner tubes in CVD prepared double wall carbon nanotubes. *Chem. Phys. Lett.*, 413:506–511, 2005.

[45] B. C. Liu, S. C. Lyu, S. I. Jung, H. K. Kang, C.-W. Yang, J. W. Park, Park C.Y., and C. J. Lee. Single-walled carbon nanotubes produced by catalytic chemical vapor deposition of acetylene over FeMo/MgO catalyst. *Chem. Phys. Lett.*, 383:104–108, 2004.

[46] Masatoshi Abe, Hiromichi Kataura, Hiroshi Kira, Takeshi Kodama, Shinzo Suzuki, Yohji Achiba, Ken-ichi Kato, Masaki Takata, Akiohiko Fujiwara, Kazuyuki Matsuda, and Yutaka Maniwa. Structural transformation from single-wall to double-wall carbon nanotube bundles. *Phys. Rev. B*, 68:041405(R), 2003.

[47] V. Zólyomi and J. Kürti. First-principles calculations for the electronic band structures of small diameter single-wall carbon nanotubes. *Phys. Rev. B*, 70:085403–1–8, 2004.

[48] M. Endo, H. Muramatsu, T. Hayashi, Y. A. Kim, M. Terrones, and M. S. Dresselhaus. Nanotechnology: ‘buckypaper’ from coaxial nanotubes. *Nature*, 433:476, 2005.

[49] F. Simon, Á. Kukovecz, C. Kramberger, R. Pfeiffer, F. Hasi, H. Kuzmany, and H. Kataura. Diameter selective characterization of single-wall carbon nanotubes. *Phys. Rev. B*, 71:165439–1–5, 2005.

[50] H. Kuzmany. *Solid-State Spectroscopy, An Introduction*. Springer Verlag, Berlin, 1998.

[51] F. Simon, Ch. Kramberger, R. Pfeiffer, H. Kuzmany, J. Zólyomi, V. Kürti, P. M. Singer, and H. Alloul. Isotope Engineering of Carbon Nanotube Systems. *Phys. Rev. Lett.*, 95:017401–1–4, 2005.

[52] J. Kürti, G. Kresse, and H. Kuzmany. First-principles calculations of the radial breathing mode of single-wall carbon nanotubes. *Phys. Rev. B*, 58:R8869–R8872, 1998.

[53] R. Pfeiffer, H. Kuzmany, T. Pichler, H. Kataura, Y. Achiba, M. Melle-Franco, and F. Zerbetto. Electronic and mechanical coupling between guest and host in carbon peapods. *Phys. Rev. B*, 69:035404, 2004.

[54] R. Pfeiffer, F. Simon, H. Kuzmany, and V. N. Popov. Fine structure of the radial breathing mode of double-wall carbon nanotubes. *Phys. Rev. B*, 72:161404–1–4, 2005.

[55] M. S. Dresselhaus, G. Dresselhaus, and Ph. Avouris. *Carbon Nanotubes: Synthesis, Structure, Properties, and Applications*. Springer, Berlin, Heidelberg, New York, 2001.

[56] H. Kataura, Y. Kumazawa, Y. Maniwa, I. Umezu, S. Suzuki, Y. Ohtsuka, and Y. Achiba. Optical properties of single-wall carbon nanotubes. *Synthetic Met.*, 103:2555–2558, 1999.

[57] R. Pfeiffer, Ch. Kramberger, F. Simon, H. Kuzmany, V. N. Popov, and H. Kataura. Interaction between concentric Tubes in DWCNTs. *Eur. Phys. J. B*, 42:345–350, 2004.

[58] V. N. Popov and Luc Henrard. Breathing-like phonon modes of multiwalled carbon nanotubes. *Phys. Rev. B*, 65:235415, 2002.

[59] A. Jorio, R. Saito, J. H. Hafner, C. M. Lieber, M. Hunter, T. McClure, G. Dresselhaus, and M. S. Dresselhaus. Structural (n, m) Determination of Isolated Single-Wall Carbon Nanotubes by Resonant Raman Scattering. *Phys. Rev. Lett.*, 86:1118–1121, 2001.

[60] Andreas Thess, Roland Lee, Pavel Nikolaev, Hongjie Dai, Pierre Petit, Jerome Robert, Chunhui Xu, Young Hee Lee, Seong Gon Kim, Andrew G. Rinzler, Daniel T. Colbert, Gustavo E. Scuseria, David Tománek, John E. Fischer, and Richard E. Smalley. Crystalline Ropes of Metallic Carbon Nanotubes. *Science*, 273:483–487, 1996.

[61] F. Simon, R. Pfeiffer, and H. Kuzmany. Temperature dependence of optical excitation lifetime and band-gap in chirality assigned semiconducting single-wall carbon nanotubes. *Phys. Rev. B*, 74:121411(R)–1–4, 2006.

[62] H. Kuzmany, W. Plank, M. Hulman, Ch. Kramberger, A. Grüneis, Th. Pichler, H. Peterlik, H. Kataura, and Y. Achiba. Determination of SWCNT diameters from the Raman response of the radial breathing mode. *Eur. Phys. J. B*, 22(3):307–320, 2001.

[63] Nachiket R. Raravikar, Pawel Keblinski, Apparao M. Rao, Mildred S. Dresselhaus, Linda S. Schadler, and Pulickel M. Ajayan. Temperature dependence of radial breathing mode Raman frequency of single-walled carbon nanotubes. *Phys. Rev. B*, 66:235424–1–9, 2002.

[64] Ch. Kramberger, R. Pfeiffer, H. Kuzmany, V. Zólyomi, and J. Kürti. Assignment of chiral vectors in carbon nanotubes. *Phys. Rev. B*, 68:235404, 2003.

[65] Brian W. Smith and David E. Luzzi. Formation mechanism of fullerene peapods and coaxial tubes: a path to large scale synthesis. *Chem. Phys. Lett.*, 321:169–174, 2000.

[66] X. Liu, T. Pichler, M. Knupfer, M. S. Golden, J. Fink, H. Kataura, Y. Achiba, K. Hirahara, and S. Iijima. Filling factors, structural, and electronic properties of C_{60} molecules in single-wall carbon nanotubes. *Phys. Rev. B*, 65:045419–1–6, 2002.

[67] F. Hasi, F. Simon, and H. Kuzmany. Reversible Hole Engineering for Single-Wall Carbon Nanotubes. *J. Nanosci. Nanotechnol.*, 5:1785–1791, 2005.

[68] Y. Zhao, B. I. Yakobson, and R. E. Smalley. Dynamic Topology of Fullerene Coalescence. *Phys. Rev. Lett.*, 88:185501–1–4, 2002.

[69] S. W. Han, M. Yoon, S. Berber, N. Park, E. Osawa, J. Ihm, and D. Tománek. Microscopic mechanism of fullerene fusion. *Phys. Rev. B*, 70:113402–1–4, 2004.

[70] J. Bardeen, L. N. Cooper, and J. R. Schrieffer. Theory of Superconductivity. *Phys. Rev.*, 108:1175–1204, 1957.

[71] F. Simon and H. Kuzmany. Growth of single-wall carbon nanotubes from ^{13}C isotope labelled organic solvents inside single wall carbon nanotube hosts. *Chem. Phys. Lett.*, 425:85–88, 2006.

[72] G. Kresse and D. Joubert. From ultrasoft pseudopotentials to the projector augmented-wave method. *Phys. Rev. B*, 59:17581775, 1999.

[73] A. S. Claye, N. M. Nemes, A. Jánossy, and J. E. Fischer. Structure and electronic properties of potassium-doped single-wall carbon nanotubes. *Phys. Rev. B*, 62:4845–4848 (R), 2000.

[74] J.-P. Salvetat, T. Fehér, C. LHuillier, F. Beuneu, and L. Forró. Anomalous electron spin resonance behavior of single-walled carbon nanotubes. *Phys. Rev. B*, 72:075440–1–6, 2005.

[75] T. Almeida Murphy, Th. Pawlik, A. Weidinger, M. Hhne, R. Alcala, and J.-M. Spaeth. *Phys. Rev. Lett.*, 77:1075, 1996.

[76] M. Waiblinger, K. Lips, W. Harneit, A. Weidinger, E. Dietel, and A. Hirsch. Thermal stability of the endohedral fullerenes N@C₆₀, N@C₇₀, and P@C₆₀. *Phys. Rev. B*, 64:159901–1–4, 2001.

[77] B. Pietzak, M. Waiblinger, T.A. Murphy, A. Weidinger, M. Hohne, E. Dietel, and A. Hirsch. *Chem. Phys. Lett.*, 279:259, 1997.

[78] A. Jánossy, S. Pekker, F. Fülöp, F. Simon, and G. Oszlányi. In *Proceedings of the IWEPNM*, page 199, 2000.

[79] X.-P. Tang, A. Kleinhammes, H. Shimoda, L. Fleming, K. Y. Bennoune, S. Sinha, C. Bower, O. Zhou, and Y. Wu. Electronic Structures of Single-Walled Carbon Nanotubes Determined by NMR. *Science*, 288:492, 2000.

[80] K.-P. Dinse. EPR investigation of atoms in chemical traps. *Phys. Chem. Chem. Phys.*, 4:5442, 2002.

[81] J. C. Hummelen, B. Knight, J. Pavlovich, R. Gonzalez, and F. Wudl. Isolation of the Heterofullerene C₅₉N as Its Dimer (C₅₉N)₂. *Science*, 269:1554–1556, 1995.

[82] J. C. Hummelen, C. Bellavia-Lund, and F. Wudl. *Heterofullerenes*, volume 199, page 93. Springer, Berlin, Heidelberg, 1999.

[83] M. J. Butcher, F. H. Jones, P. H. Beton, P. Moriarty, B. N. Cotier, M. D. Upward, K. Prassides, K. Kordatos, N. Tagmatarchis, F. Wudl, V. Dhanak, T. K. Johal, C. Crotti, C. Comicioli, and C. Ottaviani. C₅₉N Monomers: Stabilization through Immobilization. *Phys. Rev. Lett.*, 83:3478–3481, 1999.

[84] F. Fülöp, A. Rockenbauer, F. Simon, S. Pekker, L. Korecz, S. Garaj, and A. Jánossy. Azafullerene C₅₉N, a Stable Free Radical Substituent in Crystalline C₆₀. *Chem. Phys. Lett.*, 334:223, 2001.

[85] F. Simon, H. Kuzmany, J. Bernardi, F. Hauke, and A. Hirsch. Encapsulating C₅₉N azafullerene derivatives inside single-wall carbon nanotubes. *Carbon*, 44:1958–1962, 2006.

[86] A. Hirsch and B. Nuber. Nitrogen heterofullerenes. *Acc. Chem. Res.*, 32:795–804, 1999.

[87] H. Kuzmany, W. Plank, J. Winter, O. Dubay, N. Tagmatarchis, and K. Prassides. Raman spectrum and stability of (C₅₉N)₂. *Phys. Rev. B*, 60:1005–1012, 1999.

[88] P. M. Singer, P. Wzietek, H. Alloul, F. Simon, and H. Kuzmany. NMR Evidence for Gapped Spin Excitations in Metallic Carbon Nanotubes. *Phys. Rev. Lett.*, 95:236403–1–4, 2005.

[89] F. Simon, H. Kuzmany, B. Náfrádi, T. Fehér, L. Forró, F. Fülöp, A. Jánossy, A. Rockenbauer, L. Korecz, F. Hauke, and A. Hirsch. Magnetic fullerenes inside single-wall carbon nanotubes. *Phys. Rev. Lett.*, 97:136801–1–4, 2006.

[90] A. Rockenbauer, G. Csányi, F. Fülöp, S. Garaj, L. Korecz, R. Lukács, F. Simon, L. Forró, S. Pekker, and A. Jánossy. Electron delocalization and dimerization in solid C₅₉N doped C₆₀ fullerene. *Phys. Rev. Lett.*, 94:066603, 2005.

[91] F. Simon, D. Arčon, N. Tagmatarchis, S. Garaj, L. Forró, and K. Prassides. ESR signal in azafullerene (C₅₉N)₂ induced by thermal homolysis. *J. Phys. Chem. A.*, 103:6969, 1999.

[92] C. Goze-Bac, S. Latil, P. Lauginie, V. Jourdain, J. Conard, L. Duclaux, A. Rubio, and P. Bernier. Magnetic interactions in carbon nanostructures. *Carbon*, 40:1825–1842, 2002.

[93] F. Simon, R. Pfeiffer, C. Kramberger, M. Holzweber, and H. Kuzmany. *The Raman response of double wall carbon nanotubes*, pages 203–224. Springer New York, 2005.

[94] J. Kürti, V. Zólyomi, M. Kertész, and S. Guangyu. The geometry and the radial

breathing mode of carbon nanotubes: beyond the ideal behaviour. *New. J. Phys.*, 5:125.1125.21, 2003.

[95] M. A. L. Marques, M. d'Avezac, and F. Mauri. Magnetic response of carbon nanotubes from ab initio calculations, 2006.

[96] C. P. Slichter. *Principles of Magnetic Resonance*. Springer-Verlag, New York, 3rd ed. 1996 edition, 1989.

[97] H. Shimoda, B. Gao, X. P. Tang, A. Kleinhammes, L. Fleming, Y. Wu, and O. Zhou. Lithium Intercalation into Opened Single-Wall Carbon Nanotubes: Storage Capacity and Electronic Properties. *Phys. Rev. Lett.*, 88:15502, 2002.

[98] A. Kleinhammes, S.-H. Mao, X.-J. Yang, X.-P. Tang, H. Shimoda, J. P. Lu, O. Zhou, and Y. Wu. Gas adsorption in single-walled carbon nanotubes studied by NMR. *Phys. Rev. B*, 68:75418–1–6, 2003.

[99] S. Okada and A. Oshiyama. Curvature-Induced Metallization of Double-Walled Semiconducting Zigzag Carbon Nanotubes. *Phys. Rev. Lett.*, 91:216801–1–4, 2003.

[100] T. Moriya. The Effect of Electron-Electron Interaction on the Nuclear Spin Relaxation in Metals. *J. Phys. Soc. Jpn.*, 18:516, 1963.

[101] Jian Ping Lu. Novel Magnetic Properties of Carbon Nanotubes. *Phys. Rev. B*, 74:1123, 1995.

[102] C.L. Kane and E.J. Mele. Size, Shape, and Low Energy Electronic Structure of Carbon Nanotubes. *Phys. Rev. Lett.*, 78:1932–1935, 1997.

[103] J.W. Mintmire and C.T. White. Universal Density of States for Carbon Nanotubes. *Phys. Rev. Lett.*, 81:2506, 1998.

[104] H. Yoshioka. NMR relaxation rate in metallic carbon nanotubes. *J. Phys. Chem. Solids.*, 63:1281, 2002.